Please cite this article in press as: Yoon et al., Biallelic *BRF2* mutations disrupt redox homeostasis as etiological factors in syndromic immunodeficiency and developmental disorders, Molecular Therapy (2025), https://doi.org/10.1016/j.ymthe.2025.08.006

Molecular Therapy
Original Article

Biallelic *BRF2* mutations disrupt redox homeostasis as etiological factors in syndromic immunodeficiency and developmental disorders

Seobin Yoon,[1,11] Seungbok Lee,[2,3,11] Haeyoon Kwon,[4,11] Hyo-Seung Kim,[1] Jeong H. Joo,[1] Soogil Hong,[1] Soo Yeon Kim,[2,3] Sesong Jang,[3] Hyunju Lee,[5] Hyoung Soo Choi,[5] Anna Cho,[5] Soyoung Jeong,[6] Christine Suh-Yun Joh,[6] Hyeonseo Oh,[4] Eui-Hwan Choi,[7] Murim Choi,[4] Kangmo Ahn,[8,9] Hyun Je Kim,[6,10] Keun Pil Kim,[1] and Jong-Hee Chae[2,3]

[1]Department of Life Science, Chung-Ang University, Seoul, Republic of Korea; [2]Department of Genomic Medicine, Seoul National University Hospital, Seoul, Republic of Korea; [3]Department of Pediatrics, Seoul National University College of Medicine, Seoul National University Children's Hospital, Seoul, Republic of Korea; [4]Department of Medicine, Seoul National University College of Medicine, Seoul, Republic of Korea; [5]Department of Pediatrics, Seoul National University Bundang Hospital, Seongnam, Republic of Korea; [6]Department of Biomedical Sciences, Seoul National University Graduate School, Seoul, Republic of Korea; [7]Department of Biotechnology, Korea National University of Transportation, Chungju, Chungbuk, Republic of Korea; [8]Department of Pediatrics, Samsung Medical Center, Sungkyunkwan University School of Medicine, Seoul, Republic of Korea; [9]Department of Health Sciences and Technology, Samsung Advanced Institute for Health Sciences & Technology, Seoul, Republic of Korea; [10]Genomic Medicine Institute, Seoul National University College of Medicine, Seoul, Republic of Korea

TFIIB-related factor 2 (BRF2) is a critical component in the recruitment of RNA polymerase III (RNA Pol III) to type III promoters containing a TATA box. These promoters regulate the expression of key elements such as U6 spliceosomal RNA, the tRNA processing enzyme RNase P, and selenocysteine tRNA. Despite the essential role of BRF2, the genetic disorders associated with *BRF2* mutations and their molecular pathogenesis remain poorly defined. In this study, we identified and characterized novel biallelic *BRF2* variants with impaired RNA Pol III activity in a familial case presenting with multisystem anomalies, malignancy, and primary immunodeficiency. Whole-exome sequencing revealed compound heterozygous *BRF2* variants predicted to disrupt interaction with the TATA box-binding protein. Subsequent gene expression profiling of the patient's whole blood cells using single-cell RNA sequencing was conducted. Clinically, the patient exhibited recurrent infections and hypogammaglobulinemia in early childhood, which improved over time but was followed by the development of low-grade B cell lymphoma during adolescence, necessitating chemotherapy. Functional analyses in human cells expressing the *BRF2* variants demonstrated defective BRF2-dependent RNA Pol III transcription of redox-regulating genes, specifically *GPX1* and *GPX4*. These findings establish a pathogenic link between BRF2 dysfunction and disrupted redox homeostasis, offering mechanistic insights into the hemato-immunological and developmental abnormalities observed in affected individuals and highlighting potential implications for clinical management.

INTRODUCTION

The regulation of gene expression is fundamental to the intricate processes of human development, with each gene contributing critically to cellular architecture and function.[1] Among the core elements of this regulatory network is RNA polymerase III (RNA Pol III), a specialized transcriptional complex responsible for synthesizing a distinct subset of genes essential for cellular viability and homeostasis.[2–4] These transcriptional targets include transfer RNAs (tRNAs), indispensable for protein synthesis, as well as other small noncoding RNAs that support diverse cellular processes.[5,6] The coordinated interplay among RNA Pol III subunits facilitates tight regulation of this transcriptional machinery.[7] Within this framework, a key RNA Pol III-specific transcription factor (TF), TFIIB-related factor 2 (BRF2), plays an essential role in directing RNA Pol III to type III promoters, thereby enabling the expression of crucial noncoding RNAs such as U6 spliceosomal RNA, selenocysteine (SeCys) tRNA, and RNY1–5. This transcriptional activity is vital for maintaining cellular homeostasis, particularly through its involvement in redox regulation. SeCys tRNA is necessary for the biosynthesis of selenoproteins, many of which are integral to detoxifying reactive oxygen species (ROS) and preserving redox balance. Perturbations in BRF2 expression—especially its upregulation—have been shown to disrupt this balance, resulting in aberrant gene expression profiles and contributing to the pathogenesis and progression of several malignancies.[8,9] In addition, BRF2 has been

Received 26 December 2024; accepted 5 August 2025;
https://doi.org/10.1016/j.ymthe.2025.08.006.

[11]These authors contributed equally

Correspondence: Keun P. Kim, PhD, Department of Life Science, Chung-Ang University, Seoul, Republic of Korea.
E-mail: kpkim@cau.ac.kr
Correspondence: Jong-Hee Chae, MD, PhD, Department of Genomic Medicine, Seoul National University Hospital, Seoul, Republic of Korea.
E-mail: chaeped1@snu.ac.kr

Please cite this article in press as: Yoon et al., Biallelic *BRF2* mutations disrupt redox homeostasis as etiological factors in syndromic immunodeficiency and developmental disorders, Molecular Therapy (2025), https://doi.org/10.1016/j.ymthe.2025.08.006

directly implicated in modulating cellular responses to oxidative stress, influencing redox sensitivity and resistance, as demonstrated in lung adenocarcinoma models.[2] Collectively, these findings position BRF2 as a redox-sensitive transcriptional regulator that integrates RNA Pol III-mediated gene expression with oxidative stress signaling pathways.

Notably, *BRF1*, a homologous gene to *BRF2*, encodes another core component of the RNA Pol III transcriptional machinery. Pathogenic variants in *BRF1* cause cerebellofaciodental syndrome (MIM: 616202), a neurodevelopmental disorder characterized by cognitive impairments, craniofacial dysmorphisms, and dental anomalies.[10] Both BRF1 and BRF2 cooperate with the TATA binding protein (TBP) and BDP1 to form the transcription initiation complex required for RNA Pol III-mediated transcription of noncoding RNAs.[11] The clinical significance of this complex is further underscored by disease-causing mutations in its associated components: *TBP* mutations are implicated in spinocerebellar ataxia 17 (MIM: 607136), and biallelic mutations in *BDP1* are linked to congenital deafness (MIM: 618257). While BRF2 has garnered increasing attention for its role in cancer biology, no inherited disorders have thus far been definitively attributed to *BRF2* mutations.

The identification of biallelic *BRF2* variants in an individual provides critical insight into the molecular mechanisms driving complex phenotypic manifestations. These mutations impair RNA Pol III activity at type III promoters, leading to transcriptional dysregulation that contributes to delayed cellular progression and reduced expression of redox-regulating proteins. In this study, we investigate the molecular basis of genetic disorders arising from *BRF2* mutations using cultured human cells as a model system to explore the downstream molecular and cellular consequences. A central focus of this investigation is the expression of redox-associated proteins, particularly the glutathione peroxidases GPX1 and GPX4, in the context of BRF2 dysfunction.[2] GPX enzymes play a pivotal role in cellular defense against oxidative stress by neutralizing ROS and preserving redox equilibrium.[12,13] Disruption of this balance has been implicated in a range of pathological conditions, including neurodegenerative diseases, malignancies, and developmental disorders.[14–16] Importantly, the phenotypic spectrum associated with biallelic *BRF2* mutations includes diverse clinical features such as immunological dysfunction and developmental delay, emphasizing the broad physiological consequences of these genetic aberrations. Primary immunodeficiency disorders—characterized by defective or absent immune function—render individuals highly susceptible to recurrent infections, dysregulated inflammatory responses, autoimmunity, and increased risk of malignancy.[17–19] The co-occurrence of developmental delay and primary immunodeficiency presents significant clinical challenges, necessitating a comprehensive understanding of the genetic drivers of these disorders.[17–22] This study aims to delineate the relationship between *BRF2* mutations and redox protein gene expression, with the overarching goal of elucidating the molecular basis for syndromic immunodeficiency resulting from RNA Pol III dysfunction at type III promoters.[11,22] Employing a multidisciplinary approach that integrates advanced genetic analyses, molecular and cellular biology techniques, and physiological assessments, we seek to define the precise pathophysiological mechanisms by which biallelic *BRF2* mutations impair RNA Pol III-mediated transcription and disrupt downstream biological pathways. This comprehensive strategy enables the mapping of molecular alterations to defects in redox regulation, immune function, and developmental biology, offering mechanistic insight into the multifaceted clinical presentations observed in affected individuals. Ultimately, this study not only advances the understanding of *BRF2*-associated pathogenesis but also informs the development of therapeutic strategies targeting RNA Pol III-regulated pathways implicated in genetic disorders.

RESULTS

Clinical characteristics

The patient was delivered via Cesarean section at 37+1 week of gestation, with a birth weight of 2.215 kg, and presented with multiple congenital anomalies. Postnatal physical examination revealed polydactyly of the right fifth toe, which was surgically corrected (Figure 1A). At 2 months of age, the patient underwent corrective surgery for a duplex kidney on the right side (Figure 1B). Additional dysmorphic features included a prominent forehead, hypertelorism, and downslanting palpebral fissures (Figure 1C). As the patient grew older, hypodontia became evident, with seven permanent teeth, including both molars, absent due to abnormal dentition.

At 4 months of age, the patient was admitted to Seoul National University Hospital (SNUH) with a prolonged febrile illness and persistent respiratory symptoms lasting over 1 month. Immunological evaluation demonstrated reduced levels of CD19 and immunoglobulin (Ig)G/A/M, consistent with a diagnosis of primary immunodeficiency, prompting the initiation of monthly intravenous immunoglobulin (IVIG) therapy. At 6 months, the patient developed tachypnea and fever, and chest computed tomography (CT) revealed bilateral peribronchial pneumonic infiltrates (Figure 1D). Microbiologic investigations suggested concurrent *Pneumocystis jirovecii* pneumonia and cytomegalovirus (CMV) infection, with both *P. jirovecii* PCR and urinary CMV antigen tests returning positive results, and a CMV viral load of 166 copies/mL. IVIG was discontinued at 10 months of age; however, the patient required multiple subsequent hospitalizations at SNUH for recurrent pneumonia (at 24 and 37 months) and pneumococcal meningitis (at 26 and 31 months). Serial measurements of IgG/A/M consistently showed persistently low IgM levels, remaining below 40 in most assessments. Febrile seizures accompanied each episode of meningitis. IVIG therapy was reinitiated and maintained with regular monitoring of Ig levels until the patient reached 12 years of age.

Developmentally, the patient achieved independent ambulation by 12 months and exhibited no overt delays during early childhood. Brain MRI conducted at 6 months revealed a mega cisterna magna and mildly enlarged extra-axial spaces without parenchymal

Please cite this article in press as: Yoon et al., Biallelic *BRF2* mutations disrupt redox homeostasis as etiological factors in syndromic immunodeficiency and developmental disorders, Molecular Therapy (2025), https://doi.org/10.1016/j.ymthe.2025.08.006

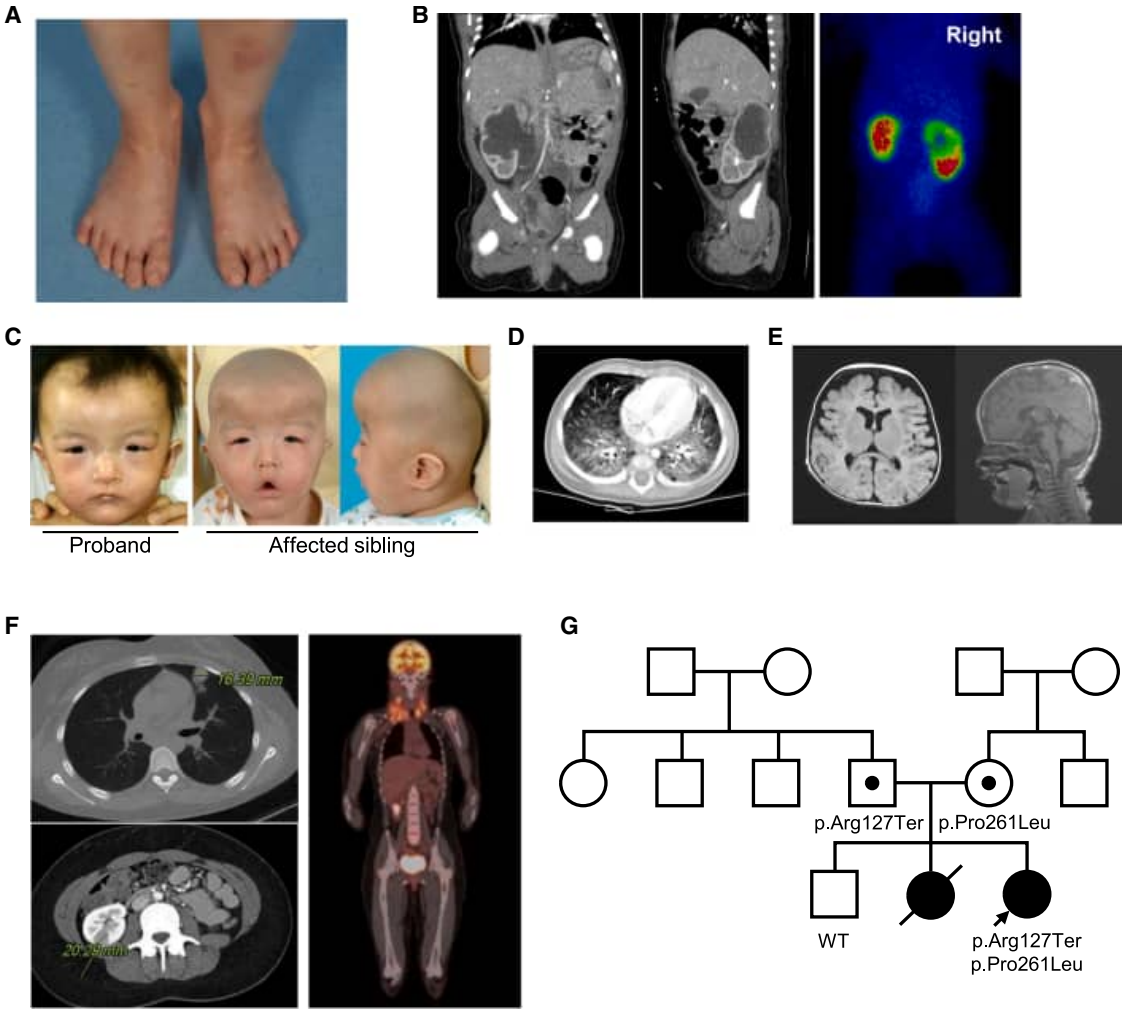

Figure 1. Clinical features of the patient with the biallelic *BRF2* mutations

(A) The patient presented with polydactyly of the right fifth toe. (B) A duplex kidney was identified on the right side, as shown in abdominal CT and PET scan images. (C) Dysmorphic facial features of the proband and her affected sibling, who passed away at 19 months of age due to *Pseudomonas* sepsis. (D) At 6 months of age, the patient developed pneumonia, with chest CT revealing diffuse ground-glass opacities along the bronchovascular bundles. (E) Brain MRI findings at 6 months of age revealed no significant abnormalities in the brain parenchyma. (F) Multifocal patchy consolidations were observed in both lungs, and a 2-cm nodule was detected in the lower pole of the right kidney. Additionally, hypermetabolic multiple lymph node enlargements were observed in the PET-CT scan. (G) Pedigree and *BRF2* mutation status of the patient and her family members.

abnormalities (Figure 1E). Two electroencephalograms, performed before the age of 3 years, were within normal limits. However, academic difficulties became evident during the patient's middle and high school years, with the patient consistently performing in the lower percentiles of her class. At 16 years of age, neurocognitive evaluation revealed a full-scale intelligence quotient of 60, consistent with mild intellectual disability.

Following the cessation of IVIG therapy, the patient did not experience severe infections; however, chronic cervical lymphadenitis persisted, necessitating repeated courses of antibiotics for exacerbations. At 13 years of age, she presented to the SNUH clinic with right cervical lymphadenopathy. Subsequent CT imaging revealed multifocal patchy consolidations in both lungs, as well as enlargement of right axillary, subclavian, lower neck, and mediastinal lymph nodes (Figure 1F). A 2-cm nodule was also identified in the lower pole of the right kidney. All lesions demonstrated hypermetabolic activity on positron emission tomography (PET)-CT. Histopathological examination of the lymph nodes confirmed the diagnosis of low-grade B cell lymphoma. The patient underwent chemotherapy and has remained in remission for over 1 year, with no evidence of disease recurrence. Additionally, she was diagnosed with autoimmune thyroiditis at age 8 and has since been maintained on levothyroxine for subclinical hypothyroidism.

Please cite this article in press as: Yoon et al., Biallelic *BRF2* mutations disrupt redox homeostasis as etiological factors in syndromic immunodeficiency and developmental disorders, Molecular Therapy (2025), https://doi.org/10.1016/j.ymthe.2025.08.006

The patient's older sister exhibited a clinical phenotype similar to that of the proband (Table S1), presenting with multiple congenital anomalies, including craniosynostosis, cleft palate, and clubfoot. As shown in Figure 1C, both siblings shared similar facial dysmorphisms, including a prominent forehead, hypertelorism, and downslanting palpebral fissures. The sister also experienced recurrent pneumonia beginning in infancy and ultimately died of *Pseudomonas* sepsis at 19 months of age, likely attributable to a congenital immunodeficiency. In contrast, the patient's older brother remains healthy, with no history of recurrent infections or congenital anomalies.

Identification of biallelic *BRF2* variants

Two rare, non-silent variants in the *BRF2* gene were identified in the patient (Figure 1G): a paternally inherited nonsense variant (c.379C>T, p.Arg127Ter) and a maternally inherited missense variant (c.782C>T, p.Pro261Leu). To detect potential pathogenic alterations not captured by whole-exome sequencing, whole-genome sequencing was performed. However, no additional pathogenic candidates were identified apart from the compound heterozygous *BRF2* variants. The combined annotation-dependent depletion (CADD) scores for the nonsense and missense variants were 36.0 and 26.7, respectively.[23] Notably, neither variant has been reported in the homozygous state in the Genome Aggregation Database (gnomAD) or Bravo (https://bravo.sph.umich.edu/) database (see Table S2). Further screening of our in-house database, which includes genotype information from more than 7,500 exomes and 5,000 genomes from patients with rare diseases and their family members, also revealed no individuals carrying these variants in a compound heterozygous or homozygous state, except for the proband.[24]

In the gnomAD database (version 4.1.0), 97 predicted loss-of-function (pLoF) variants were identified in the *BRF2* gene, with allele frequencies ranging from 6.19×10^{-7} to 9.67×10^{-5}.[25] Although 30.8 pLoF variants were expected based on statistical models, only 17 were observed, yielding an observed-to-expected ratio of 0.55 (90% confidence interval: 0.38–0.83). Notably, none of the identified variants were present in the homozygous state. Similarly, the Bravo database listed 37 pLoF variants, with allele frequencies between 3.31×10^{-6} and 5.63×10^{-5}, and no individuals were homozygous for any of these variants. These findings underscore the rarity of the identified *BRF2* variants and support their potential pathogenicity in an autosomal recessive context. DNA samples from the patient's deceased older sister were unavailable due to her passing more than 5 years earlier at a different institution. However, genotyping of the healthy older brother confirmed that he did not carry either of the identified variants (Figure 1G).

Sequence alignment and structural analysis of BRF2

The BRF2 protein consists of four distinct domains: the Zn-ribbon/B-reader/B-linker, N-cyclin repeat, C-cyclin repeat, and the C-terminal domain (Figure 2A). *In silico* three-dimensional protein modeling was employed to localize the mutation sites within the *BRF2* structure. The Arg127 residue is situated within the N-cyclin repeat domain, while Pro261 is located in the C-cyclin repeat domain. The C-cyclin repeat domain interacts with the major groove of DNA upstream of the TATA box and forms a key interface with TBP.[2,26–28] In contrast, the N-cyclin repeat domain—analogous to the corresponding region in TFIIB—interacts with the phosphodiester backbone of DNA. To facilitate visualization of the mutations, the Arg127Ter and Pro261Leu sites were highlighted in blue and red, respectively (Figure 2A). Multiple sequence alignment of the BRF2 protein across species, including chimpanzee, rhesus monkey, rabbit, horse, dog, elephant, chicken, and frog, revealed strong evolutionary conservation (Figures 2B and S1). The Pro261 residue, in particular, demonstrated high interspecies conservation (Figure 2B). Although AlphaMissense classified the Pro261 variant as being of ambiguous pathogenicity, most substitutions at this position were predicted to be pathogenic. Additionally, the phyloP100way conservation score for this site was 7.99, supporting significant evolutionary constraint (Figure 2B). Structural modeling of the BRF2-TBP/DNA complex further revealed hydrogen bond interactions among DNA, TBP, and BRF2 in the wild-type configuration (Figure 2C). Specifically, Arg127 forms a direct interaction with TBP, while Pro261, through Tyr260, engages with the non-template DNA strand. Mutations at either Arg127 or Pro261 are therefore likely to disrupt the formation of the TFIIIB complex, leading to impaired RNA Pol III function.

Single-cell transcriptomic analysis of PBMCs from the BRF2-mutant patient and healthy controls

We performed single-cell transcriptomic profiling of peripheral blood mononuclear cells (PBMCs) obtained from the patient harboring *BRF2* mutations and four age-matched pediatric healthy controls. After quality control and the exclusion of platelet and red blood cell contaminants, a total of 42,735 high-quality cells were retained for analysis (Figure S2). To identify potential BRF2 deficiency–associated transcriptional changes, we conducted gene set enrichment analyses (GSEA) using the Kyoto Encyclopedia of Genes and Genomes, Reactome, and Gene Ontology (GO): Biological Process gene sets on the combined PBMC dataset (patient vs. controls). All significantly enriched pathways that met the criteria of adjusted $p < 0.05$ and $|\text{normalized enrichment score (NES)}| > 2$ were negatively enriched in the patient sample (i.e., NES < -2). These included selenoamino acid metabolism, and response of EIF2AK4 (GCN2) to amino acid deficiency, suggesting a marked impairment in BRF2-TFIIIB-mediated transcriptional processes (Figure 3A).

Cluster annotation based on canonical immune marker genes identified 12 major immune cell subsets, including B cells, myeloid and plasmacytoid dendritic cells, classical and non-classical monocytes, natural killer cells, plasma cells, and T cell populations (Figures 3B and S3). To determine whether the observed transcriptional deficits were confined to specific immune lineages or shared across cell types, we calculated AUCell scores for representative downregulated pathways. Patient-derived cells consistently exhibited lower AUCell scores across all major immune cell lineages, particularly in pathways impacted by tRNA deficiency, such as selenoamino acid metabolism and the GCN2-mediated amino acid starvation response (Figures 3C and S4). These results suggest that BRF2-associated RNA Pol III

Please cite this article in press as: Yoon et al., Biallelic *BRF2* mutations disrupt redox homeostasis as etiological factors in syndromic immunodeficiency and developmental disorders, Molecular Therapy (2025), https://doi.org/10.1016/j.ymthe.2025.08.006

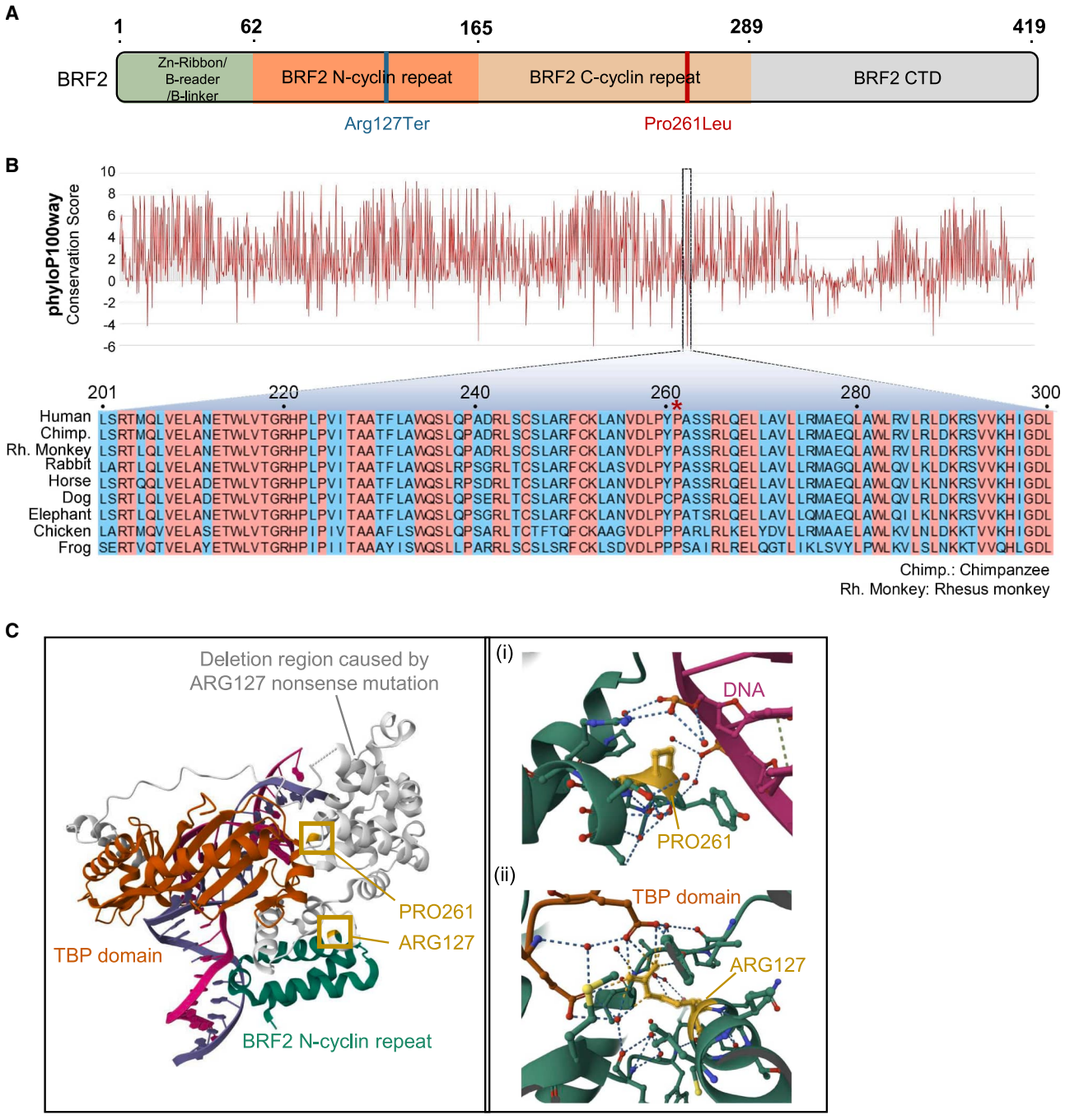

Figure 2. Sequence alignment and structural analysis of BRF2

(A) Schematic illustration of BRF2 domain organization and mutations, with the ARG127 nonsense mutation marked in blue and the PRO261 missense mutation marked in red.[2] (B) Amino acid sequence alignment across species, with the top showing phyloP scores alongside the BRF2 amino acid sequence. The 201st–300th amino acids of BRF2 are displayed, with mutation sites indicated by asterisks. Blue in the alignment indicates low conservation positions, while red denotes highly conserved amino acids. (Homo sapiens (GenBank: NM_018310) Pan troglodytes (GenBank: XM_001169914) Macaca mulatta (GenBank: XM_015145163) Oryctolagus cuniculus (GenBank: XM_002720786) Equus caballus (GenBank: XM_023630782) Canis lupus familiaris (GenBank: XM_038689903) Loxodonta africana (GenBank: XM_064272818) Gallus gallus (GenBank: XM_424383) Xenopus tropicalis (GenBank: XM_031897566).). (C) Tertiary structure of the BRF2-TBP/DNA complex, with close-up views of the PRO261 (i) and ARG127 (ii) sites.[2] The deletion region caused by the ARG127 nonsense mutation is colored white, and the dots between the DNA and protein domains represent hydrogen bond interactions (Protein Data Bank: 4ROC).

Please cite this article in press as: Yoon et al., Biallelic *BRF2* mutations disrupt redox homeostasis as etiological factors in syndromic immunodeficiency and developmental disorders, Molecular Therapy (2025), https://doi.org/10.1016/j.ymthe.2025.08.006

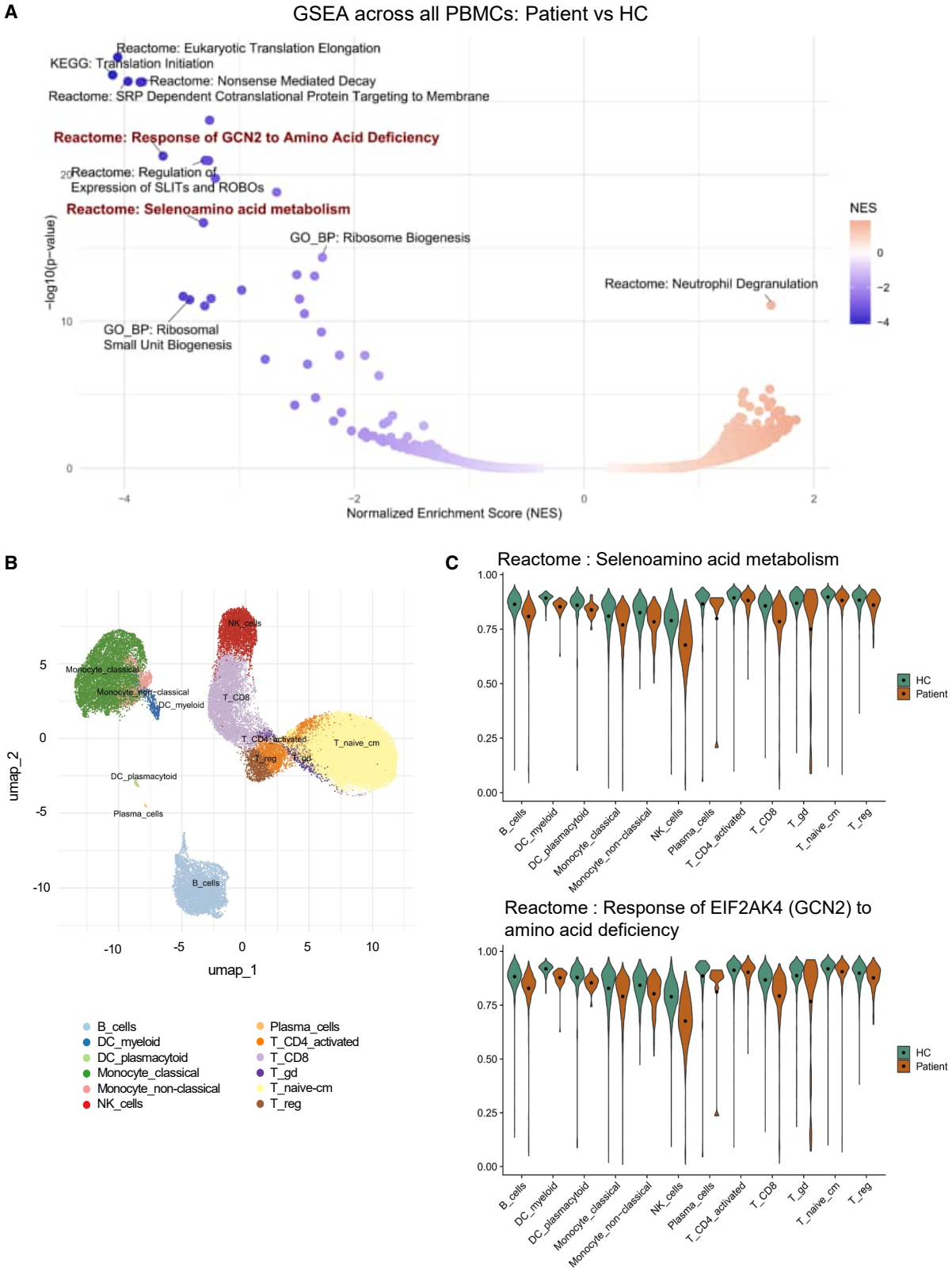

(legend on next page)

Please cite this article in press as: Yoon et al., Biallelic *BRF2* mutations disrupt redox homeostasis as etiological factors in syndromic immunodeficiency and developmental disorders, Molecular Therapy (2025), https://doi.org/10.1016/j.ymthe.2025.08.006

dysfunction exerts broad, cell-type-independent effects on immune transcriptomes at the single-cell level.

Patient-specific monocyte subset exhibits altered expression of immune and redox-related genes

To further investigate the lineage-specific consequences of BRF2 deficiency, we analyzed immune cell proportions across all individuals and found an expansion of classical monocytes in the patient, along with a relative reduction in T cell subsets (Figure 4A). Given this marked expansion, we assessed transcriptional differences between classical monocytes derived from the patient and those from healthy controls. Subclustering analysis of classical monocytes identified 8 transcriptionally distinct subsets (m1–m8). Cluster m5 was composed almost exclusively of patient-derived cells (90%), whereas cluster m7 consisted predominantly of cells from healthy controls (97%) (Figure 4B). Based on these patterns, we designated m5 and m7 as representative of patient-specific and control-like monocytes, respectively. Notably, expression of selenoprotein genes reliant on RNA Pol III-transcribed tRNAs, such as SELENOK and the oxidoreductase GPX4, were significantly reduced in m5 compared to m7 (Figure 4C). Further supporting the notion that redox regulation is impaired across immune lineages, a similar reduction in *GPX4* and *SELENOK* was also observed in a patient-specific B cell subcluster (Figure S5).

To elucidate the broader functional implications of these transcriptional changes, we conducted differential expression analysis between m5 and m7, identifying the top 40 differentially expressed genes (DEGs), which were visualized via heatmap (Figures 4D and S6). m7 (control-like) cells showed elevated expression of genes involved in chemotaxis (*CXCL3* and *CCL7*), cell adhesion (*ITGB8* and *ICAM1*), apoptosis regulation (*PHLDA1*[29] and *FTH1*[30]), and immune activation (*IL1B*, *CD83*, and *CD109*), whereas these gene modules were broadly downregulated in m5 (patient-specific) cells. Subsequent GSEA of the DEGs revealed downregulation of multiple pathways integral to monocyte function in the m5 cluster. These included pathways involved in responses to inflammatory cytokines, immune tolerance maintenance, and recruitment to peripheral tissues (Figure 4E).

Validation of gene expression changes induced by *BRF2* mutations

This study focuses on the identification and functional characterization of the biallelic *BRF2* mutants BRF2-Pro261Leu and BRF2-Arg127Ter. HEK293T cells were transfected with plasmids encoding either wild-type *BRF2* or one of the two mutant *BRF2* variants, and protein expression was confirmed via western blot analysis (Figure 5A). As BRF2 functions as a subunit of the TFIIIB complex, which is particularly active during the S and G2 phases of the cell cycle,[9,31] we first examined the effects of ectopic expression of wild-type and mutant BRF2 on cell-cycle progression in HEK293T cells (Figure 5B). Cells overexpressing BRF2 exhibited a modest increase in the S and G2 phases relative to those transfected with an empty vector; however, the overall cell-cycle distribution remained largely unchanged regardless of whether BRF2 was wild-type, missense mutated, or nonsense mutated (Figure 5B). Next, we assessed transcript levels of *GPX1*, *GPX4*, and *7SK*, which are regulated by *BRF2*-TFIIIB activity. Overexpression of wild-type *BRF2* led to a significant upregulation of these transcripts. In contrast, the BRF2 mutants (Pro261Leu and Arg127Ter) resulted in marked reductions in transcript abundance. Specifically, *GPX1* levels decreased to 0.58 ± 0.19 and 0.65 ± 0.14, *GPX4* decreased to 0.56 ± 0.19 and 0.64 ± 0.14, and *7SK* RNA decreased to 0.50 ± 0.14 and 0.62 ± 0.08, respectively (Figure 5C). These findings suggest that *BRF2* mutations impair the role of BRF2 in mediating RNA Pol III-dependent transcription at type III promoters, thereby reducing expression of its downstream gene targets. To further validate the functional role of *BRF2* in HEK293T cells, we performed *BRF2* knockdown using small interfering RNA (siRNA). Three siRNA constructs targeting *BRF2* were evaluated for knockdown efficiency (Figure 5D). *siBRF2* number 1 reduced *BRF2* expression by 28%, *siBRF2* number 2 by 84%, and *siBRF2* number 3 achieved the most robust reduction at 92% (Figure 5D). *siBRF2* number 3 was therefore selected for subsequent experiments. Upon siRNA-mediated depletion of *BRF2*, transcript levels of *GPX4* were reduced to 54% of control, *GPX1* to 52%, and *7SK* RNA to 64% (Figure 5E). These results confirm that both mutation and knockdown of *BRF2* suppress expression of *BRF2*-dependent transcripts.

BRF2-regulated gene expressions in embryonic development and genome integrity gene sets

We conducted RNA sequencing (RNA-seq) analyses on siControl- and *siBRF2*-treated cells, revealing distinct differences in gene expression profiles between the two groups (Figures 6A and 6B). DEGs were evaluated for enrichment in GO categories. Upregulated DEGs were significantly enriched in gene sets associated with transcriptional regulation (Figure 6C), with "regulation of transcription from RNA polymerase II promoter" emerging as the most enriched

Figure 3. Single-cell transcriptomic profiling of PBMCs from a *BRF2*-mutant patient compared to healthy controls

(A) GSEA of bulk PBMCs (patient vs. healthy controls). Volcano plot showing normalized enrichment scores (NESs) for gene sets significantly enriched in the patient vs. controls (adjusted $p < 0.05$). Negatively enriched pathways (left) in the patient include selenoamino acid metabolism and response of EIF2AK4 (GCN2) to amino acid deficiency, processes associated with tRNA activity. Only a limited number of pathways show positive enrichment (right). (B) Uniform manifold approximation and projection (UMAP) clustering of PBMCs. UMAP projection of integrated single-cell transcriptomic data from the *BRF2*-mutant patient and four pediatric healthy controls, colored by major immune cell types. Distinct clusters represent T cells ($CD4^+$, $CD8^+$), B cells, classical and non-classical monocytes, natural killer (NK) cells, dendritic cells (DCs), and others. (C) AUCell scores for BRF2-related downregulated pathways. Violin plots showing AUCell scores for two gene sets responsive to tRNA deficiency—Reactome: selenoamino acid metabolism and Reactome: response of EIF2AK4 (GCN2) to amino acid deficiency—across major immune cell types. Dots within violins indicate mean values calculated from log-normalized expression data. Scores are compared between the patient (orange) and healthy controls (HC; green). Across all cell types, patient cells consistently exhibit lower AUCell scores, indicating a broad impairment of BRF2/TFIIIB-dependent transcription in immune cells.

Please cite this article in press as: Yoon et al., Biallelic *BRF2* mutations disrupt redox homeostasis as etiological factors in syndromic immunodeficiency and developmental disorders, Molecular Therapy (2025), https://doi.org/10.1016/j.ymthe.2025.08.006

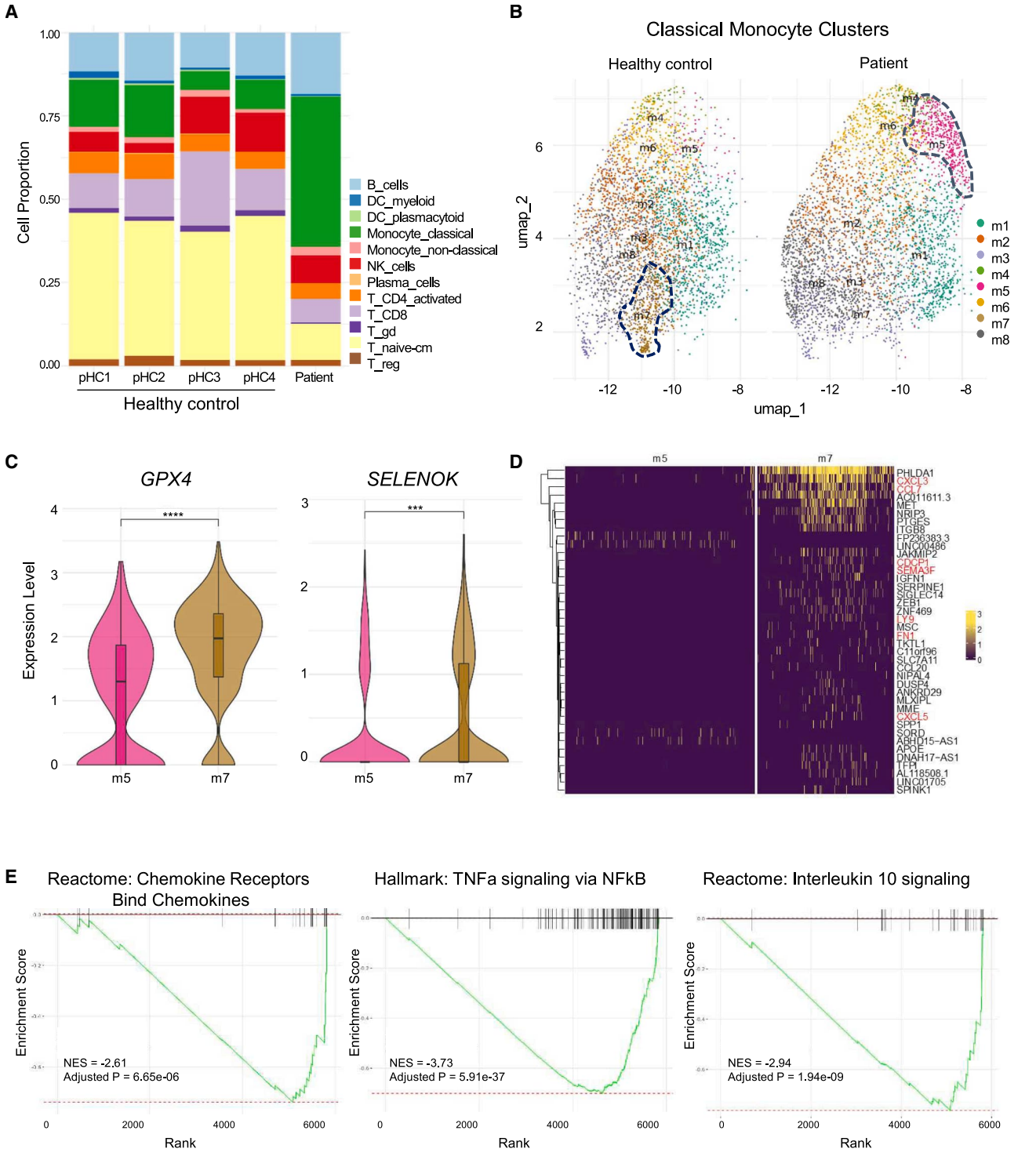

Figure 4. Analysis of classical monocyte subclusters in a *BRF2*-mutant patient and healthy controls

(A) Cell type proportions across samples. The stacked bar chart illustrates the distribution of broad immune cell types (e.g., B cells, T cells, NK cells, classical monocytes) in the patient and four HCs. The patient's PBMCs show a notably higher proportion of classical monocytes compared to controls. (B) UMAP projection of classical monocytes, depicting eight subclusters (m1–m8). Clusters are colored by m1–m8 designations. The patient-specific cluster m5 is distinguishable in the patient, whereas the m7 cluster contains predominantly HC cells. (C) Selenoprotein gene expression in classical monocyte clusters. Violin plots of *GPX4* (top) and *SELENOK* (bottom) expression in clusters

(legend continued on next page)

term (p = 9.41E−24). Additional highly ranked gene sets were associated with embryonic development, including "anterior/posterior pattern specification" (p = 1.78E−12) and "embryonic skeletal system morphogenesis" (p = 2.47E−7). In contrast, downregulated DEGs were predominantly enriched in categories related to "DNA repair" (p = 3.70E−4) and "DNA metabolic processes" (p = 3.98E−4) (Figure 6D).

BRF2 expression is reduced under redox stress

We next assessed the effect of redox stress on *BRF2* transcription, given its role as a redox-sensitive regulator of SeCys tRNA expression, which is critical for the synthesis of detoxification enzymes.[13] To examine transcript levels of *BRF2*, *GPX1*, and *GPX4* under oxidative stress conditions, HEK293T cells were treated with 600 μM *tert*-butyl hydroperoxide (tBHP) for 3 h. Cell viability declined significantly after 3 h of tBHP exposure compared to 1-h and 2-h treatments, with the 3-h duration resulting in extensive cell damage (Figure S7). Under these conditions, *BRF2* expression was reduced by approximately 66%, indicating that oxidative stress suppresses *BRF2* transcription (Figures 7A and 7B). Similarly, *GPX1* and *GPX4* transcript levels were reduced by 4% and 54%, respectively, compared to untreated HEK293T cells (Figures 7A and 7B). These findings suggest that oxidative stress inhibits *BRF2* expression and consequently downregulates the expression of key selenoproteins involved in cellular detoxification.

Overexpression of wild-type *BRF2* enhances expression of type III promoter-dependent genes, while *BRF2* mutations result in reduced viability

Previous studies by Vannini et al. demonstrated that overexpression of *BRF2* mitigates redox stress-induced reductions in SeCys tRNA levels.[2] To further elucidate *BRF2*-dependent gene regulation under redox stress conditions, cells were transfected with constructs expressing either wild-type *BRF2*, a missense *BRF2* mutant, or a nonsense *BRF2* mutant, followed by exposure to tBHP to induce oxidative stress. Protein expression of *BRF2* was confirmed via western blot analysis (Figure 7C). Transient overexpression of *BRF2* was achieved using an overexpression vector, resulting in a substantial increase in *BRF2* protein levels (Figure 7C). To assess changes in *BRF2*-dependent gene expression under oxidative stress, quantitative real-time PCR was performed in cells overexpressing *BRF2* in the presence of tBHP. Redox stress significantly decreased transcript levels of *GPX1*, *GPX4*, and *7SK* (Figure S8A). This downregulation of type III RNA Pol III-dependent genes under oxidative conditions likely results from the reduction in *BRF2* expression during redox stress (Figures 7A and 7B).

Co-expression experiments with the *BRF2* missense (Pro261Leu) and nonsense (Arg127Ter) mutants were also conducted, and expression levels of RNA Pol III-dependent genes were analyzed by quantitative real-time PCR (Figures S8B and S8C). Co-expression of the mutants led to reduced transcript levels of *GPX1*, *GPX4*, and *7SK*. However, transcript levels of these *BRF2*-dependent genes were comparable between cells expressing either BRF2-Pro261Leu or BRF2-Arg127Ter alone and those co-expressing both mutants (Figures S8B and S8C). Under basal redox conditions, *GPX1* transcript levels declined to 0.44-, 0.40-, and 0.44-fold, respectively, in cells expressing the same mutant configurations. In contrast, wild-type *BRF2* overexpression resulted in a 3.7-fold increase in *GPX1* transcript levels compared to the empty vector control (Figure S8B). *GPX4* RNA levels were 2.49-fold higher in cells overexpressing wild-type *BRF2* relative to controls, while expression was reduced by 0.5- and 0.41-fold in BRF2-Pro261Leu and BRF2-Arg127Ter-transfected cells, respectively. In co-transfected cells, the transcript level was decreased by 0.63-fold. Similarly, *7SK* transcript levels in wild-type *BRF2*-transfected cells were 1.6-fold higher than in empty vector controls (Figure S8B). Conversely, *7SK* expression was significantly reduced in cells expressing mutant *BRF2*—by 0.43-fold in BRF2-Pro261Leu, 0.35-fold in BRF2-Arg127Ter, and 0.47-fold in co-transfected cells (Figure S8B).

Under redox stress conditions, transcript levels of antioxidant genes and *7SK* were reduced in cells overexpressing either *BRF2* mutant (Figure S8C). *GPX1* expression was 1.62-fold higher in cells overexpressing wild-type *BRF2* compared to controls, whereas *GPX1* transcript levels were reduced by approximately 50% in cells expressing either mutant alone or in combination (Figure S8C).

GPX4 expression was reduced by 0.55-fold in BRF2-Pro261Leu-transfected cells, 0.62-fold in BRF2-Arg127Ter-transfected cells, and 0.56-fold in cells co-expressing both mutants. By contrast, *GPX4* transcript levels were 2.2-fold higher in cells expressing wild-type *BRF2* compared to the control group (Figure S8C). In cells transfected with the BRF2-Pro261Leu mutant, *7SK* expression was approximately 30% lower than in empty vector controls. Similarly, *7SK* transcript levels were reduced by 0.73-fold in BRF2-Arg127Ter-transfected cells and by approximately 40% in cells co-expressing both mutants (Figure S8C). In contrast, overexpression of wild-type *BRF2* resulted in a 2.85-fold increase in *7SK* transcripts relative to the empty vector (Figure S8C). These findings suggest that co-expression of BRF2-Pro261Leu and BRF2-Arg127Ter mutants results in a marked reduction in type III RNA Pol III-dependent

m5 and m7. The patient-specific cluster (m5) exhibits markedly lower expression of these selenoprotein-related genes compared to cluster m7. The central horizontal line in each violin represents the median, and statistical significance was determined using the Wilcoxon rank-sum test (p values indicated by asterisks; $p < 0.001$: ***, $p < 0.0001$: ****). (D) Heatmap of 40 top differentially expressed genes (DEGs; m5 vs. m7). Unsupervised clustering of the top DEGs (by avg_log2FC) shows that m7 (healthy-like) monocytes highly express genes involved in adhesion, chemotaxis, and apoptosis, whereas m5 (patient-like) monocytes have diminished expression of these functional markers. The color scale represents log-normalized expression values. (E) GSEA plots for Reactome: chemokine receptors bind chemokines (NES = −2.61, adjusted p < 6.5E−6), hallmark: tumor necrosis factor alpha (TNFa) signaling via nuclear factor κB (NFkB) (NES = −3.73, adjusted p < 5.91E−37), and Reactome: interleukin 10 signaling (NES = −2.94, adjusted p < 1.94E−9), indicating significant downregulation in the m5 cluster.

Please cite this article in press as: Yoon et al., Biallelic *BRF2* mutations disrupt redox homeostasis as etiological factors in syndromic immunodeficiency and developmental disorders, Molecular Therapy (2025), https://doi.org/10.1016/j.ymthe.2025.08.006

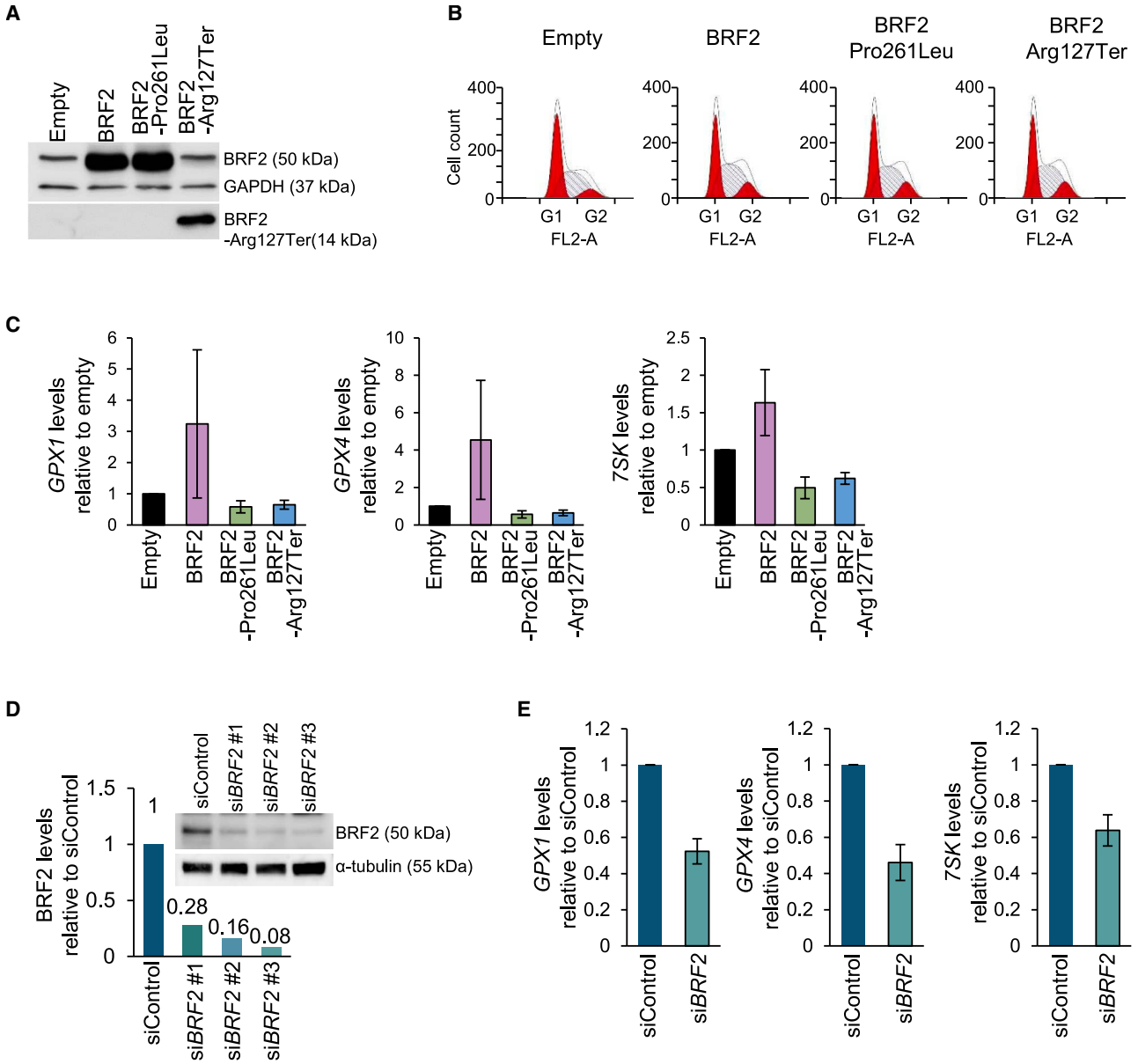

Figure 5. Gene expression change in *BRF2* mutations and depletion

(A) Overexpression of *BRF2* or *BRF2* mutants. The ectopic expression levels of *BRF2* or two types of *BRF2* mutants were determined by western blot analysis. (B) Cell-cycle pattern in *BRF2*- and *BRF2* mutant-overexpressing HEK293T cells. Cell-cycle analysis was conducted in HEK293T cells with empty vector (Empty), *BRF2* wild-type (*BRF2*), and *BRF2* mutated genes (BRF2 Pro261Leu and BRF2 Arg127Ter). (C) Effects of *BRF2* and *BRF2* mutants on gene expression. RNA levels of *BRF2*-related genes, including *GPX1*, *GPX4*, and *7SK* were determined by quantitative real-time PCR. Three independent experiments were performed, and the bar graphs indicate averages and standard deviations (SDs). (D) Depletion of *BRF2* via siRNA. Three si*BRF2* candidates were selected, and *BRF2* expression levels in *BRF2*-depleted HEK293T cells with each siRNA candidate were confirmed using immunoblot analysis. (E) Transcript levels of *BRF2*-related genes. Quantitative real-time PCR was performed to determine the RNA expression levels of *GPX1*, *GPX4*, and *7SK* in *BRF2*-depleted cells. Three independent experiments were performed, and error bars indicate the mean ± SD.

gene expression under oxidative stress. To assess whether RNA Pol III itself was affected by *BRF2* mutations under redox stress, POLR3A—a core subunit of the RNA Pol III complex—was evaluated via western blot. *POLR3A* expression remained stable regardless of *BRF2* mutation status or oxidative stress exposure (Figure S9), indicating that neither *BRF2* mutations nor redox stress significantly impact RNA Pol III protein levels.

In HEK293T cells overexpressing wild-type *BRF2*, transcript levels of *BRF2*-dependent genes increased despite the presence of oxidative

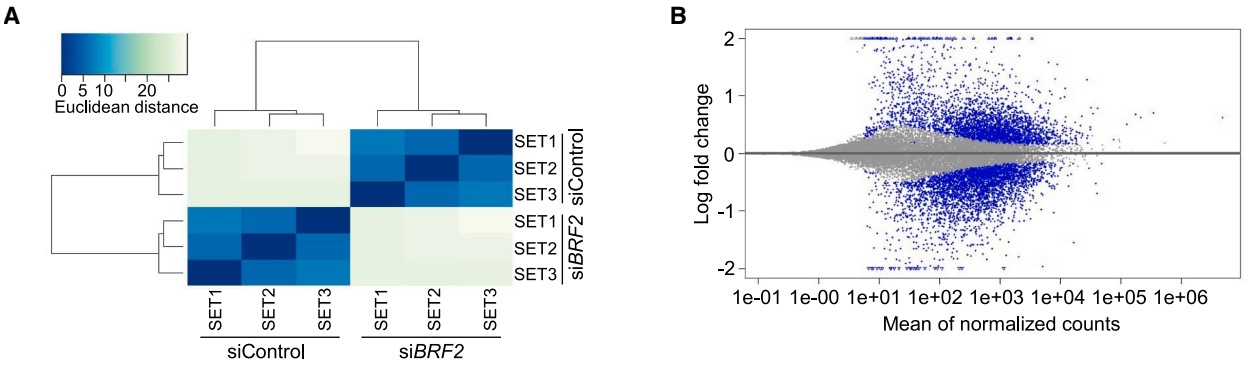

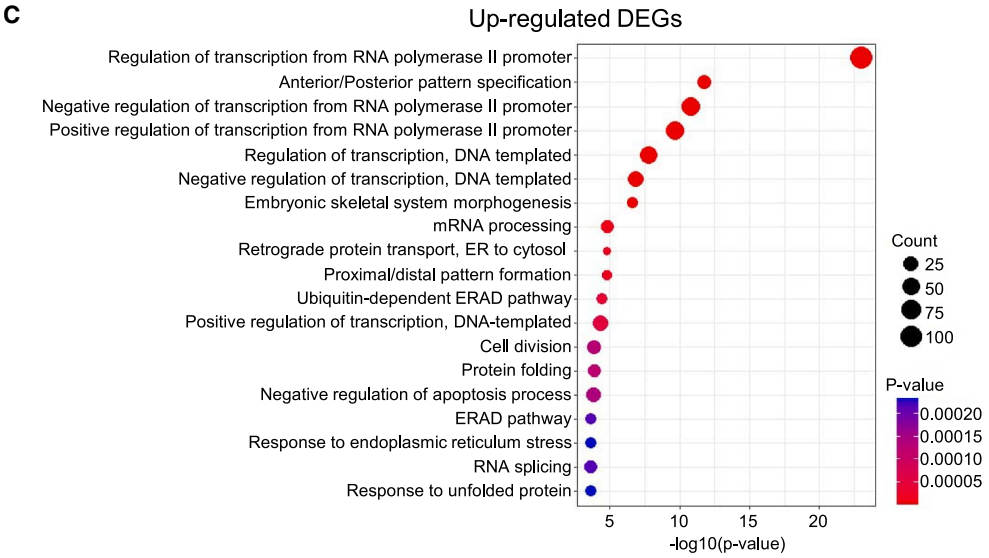

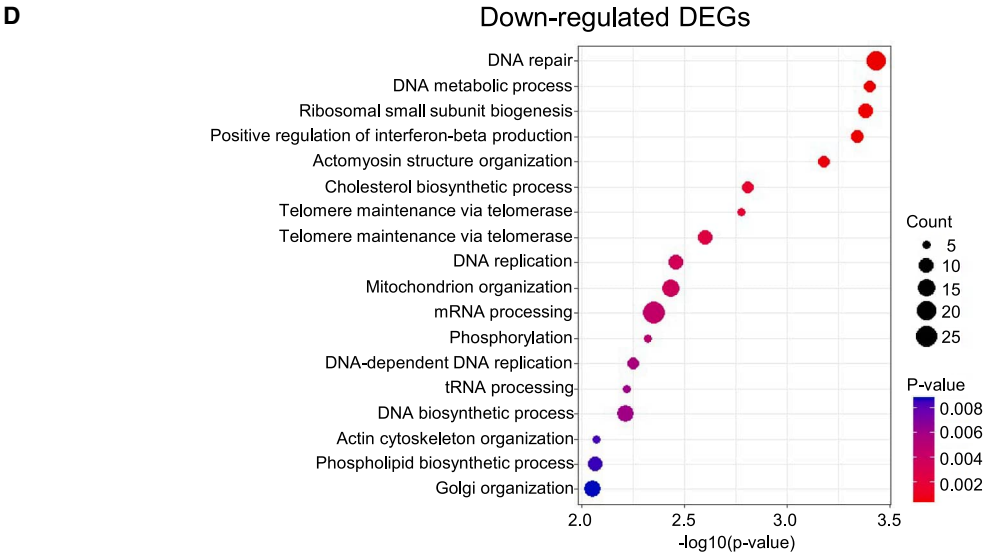

(legend on next page)

Please cite this article in press as: Yoon et al., Biallelic *BRF2* mutations disrupt redox homeostasis as etiological factors in syndromic immunodeficiency and developmental disorders, Molecular Therapy (2025), https://doi.org/10.1016/j.ymthe.2025.08.006

stress (Figure 7D). Specifically, the expression levels of *GPX1* and *GPX4* increased by approximately 1.5- and 1.8-fold, respectively, compared to cells transfected with an empty plasmid (Figure 7D), while *7SK* RNA levels increased by approximately 1.3-fold. In contrast, cells expressing *BRF2* mutants exhibited a marked reduction in transcript levels of *BRF2*-dependent genes, irrespective of the mutation type (Figure 7D). In cells overexpressing the missense mutant BRF2-Pro261Leu, *GPX1* and *GPX4* transcript levels were 0.68 ± 0.14 and 0.80 ± 0.16, respectively, relative to empty plasmid controls, and *7SK* RNA levels decreased by approximately 0.7 (Figure 7D). Similarly, in cells expressing the nonsense mutant BRF2-Arg127Ter, transcript levels of *GPX1*, *GPX4*, and *7SK* RNA were 0.71 ± 0.04, 0.74 ± 0.13, and 0.65 ± 0.04, respectively (Figure 7D). These data suggest that wild-type *BRF2* overexpression under oxidative stress rescues the expression of *BRF2*-dependent genes. To further evaluate the role of antioxidant supplementation, we examined the effect of selenium on *GPX4* expression under redox stress. Cells transfected with an empty vector, wild-type *BRF2*, or *BRF2* mutants were treated with selenium, and *GPX4* transcript levels were quantified by quantitative real-time PCR (Figure S10). Selenium treatment significantly increased *GPX4* expression under all conditions, regardless of *BRF2* mutation status. In selenium-treated cells overexpressing wild-type *BRF2*, *GPX4* levels were approximately 33-fold higher compared to empty vector-transfected cells under redox stress (Figure S10). Likewise, *GPX4* transcript levels increased by approximately 17-fold and 16-fold in cells expressing BRF2-Pro261Leu and BRF2-Arg127Ter, respectively, relative to stressed controls (Figure S10). These findings indicate that selenium treatment, in conjunction with *BRF2* overexpression, including mutated forms, can partially restore antioxidant gene expression under oxidative conditions.

We further investigated cell viability under oxidative stress. In cells transfected with an empty plasmid, viability was 29.3%, compared to 35.7% in those overexpressing wild-type *BRF2* (Figure 7E). By contrast, overexpression of *BRF2* mutants significantly reduced cell viability to 17.7% in cells expressing the missense variant and 16.1% in cells expressing the nonsense variant (Figure 7E). Notably, in the absence of oxidative stress, cell viability did not differ significantly among groups. HEK293T cells transfected with an empty vector showed 94% survival, while those expressing wild-type *BRF2* exhibited 94.4% survival, and 95%–96% of cells expressing the *BRF2* mutants survived (Figure S11A). These findings suggest that overexpression of wild-type *BRF2* under redox stress conditions restores the expression of *BRF2*-dependent genes, including selenoproteins, thereby enhancing cellular viability. In contrast, *BRF2* mutations exacerbate the deleterious effects of oxidative stress on cell survival. Finally, we assessed whether depletion of GPX4, a selenoprotein synthesized using SeCys tRNA transcribed by type III RNA Pol III, would impact *7SK* expression and cell viability. Among the siRNA constructs tested, candidate 3 (*siGPX4* number 3) demonstrated the most effective knockdown efficiency (Figure S11B). *GPX4* knockdown resulted in reduced *7SK* levels and increased cell death (Figures S11C–S11E).

In HEK293T cells treated with *siGPX4* under non-stress conditions, *7SK* transcript levels decreased to 0.74-fold relative to cells treated with a control siRNA (siControl) (Figure S11D). Under oxidative stress, *GPX4* knockdown exerted a more pronounced effect, reducing *7SK* expression to 0.18-fold compared to siControl-treated cells (Figure S11D). Regarding cell viability, 86.5% of siControl cells remained viable under baseline conditions, whereas viability decreased to 78.3% in *GPX4*-depleted cells. Under redox stress, *GPX4* knockdown significantly impaired cell survival, with only 49.7% of *siGPX4*-treated cells remaining viable, compared to 63.1% in the siControl group (Figure S11E).

Dramatic decrease in *BRF2*-dependent genes in *BRF2*-depleted cells during redox stress

Mutations that impair BRF2 function suppress RNA Pol III activity, leading to decreased transcription of *BRF2*-dependent genes, including members of the *GPX* family and *7SK* RNA. Oxidative stress further exacerbates this dysfunction by downregulating *BRF2* expression, thereby reducing antioxidant enzyme levels. To investigate *BRF2*-dependent gene expression under oxidative stress conditions, HEK293T cells were treated with tBHP and transfected with siRNA targeting *BRF2*. Redox stress alone reduced *BRF2* transcript levels to 0.58 ± 0.21, whereas combined treatment with *siBRF2* and redox stress further decreased expression to 0.40 ± 0.17 (Figure 7F). During oxidative stress, *GPX1* transcript levels were reduced to 0.39 ± 0.15 in siControl-treated cells and to 0.36 ± 0.10 in *siBRF2*-treated cells. Similarly, *GPX4* levels declined to 0.42 ± 0.19 and 0.35 ± 0.10, respectively (Figure 7F). We found that *7SK* RNA expression also decreased to approximately 51.51% in siControl-treated cells and to 42.52% in si*BRF2*-treated cells under the same conditions (Figure 7F). Under oxidative stress, BRF2 protein levels were reduced in siControl cells and nearly abolished in *BRF2*-depleted cells (Figure S12). Consistently, expression of selenoproteins, including *GPX1* and *GPX4*, was suppressed by approximately 85% upon *BRF2* inhibition in redox-stressed cells (Figure S12). These findings collectively indicate that *BRF2* depletion significantly impairs type III promoter-dependent gene expression in the context of oxidative stress, thereby increasing cellular vulnerability. Furthermore, reduced *BRF2* expression impaired cell proliferation, as reflected by decreased transcript levels of proliferation markers *PCNA* and *MCM2–10* in *BRF2*-depleted HEK293T cells

Figure 6. BRF2-regulated gene expressions in both RNA Pol II-dependent and -independent gene sets

(A) Heatmap displaying the Euclidean distances between RNA-seq samples based on sample similarity. (B) MA plot illustrating the differential expression of genes between si*BRF2*-treated and untreated samples. (C and D) Dot plots show Gene Ontology (Biological Processes) significantly enriched in upregulated (C) and downregulated (D) DEGs.

Please cite this article in press as: Yoon et al., Biallelic *BRF2* mutations disrupt redox homeostasis as etiological factors in syndromic immunodeficiency and developmental disorders, Molecular Therapy (2025), https://doi.org/10.1016/j.ymthe.2025.08.006

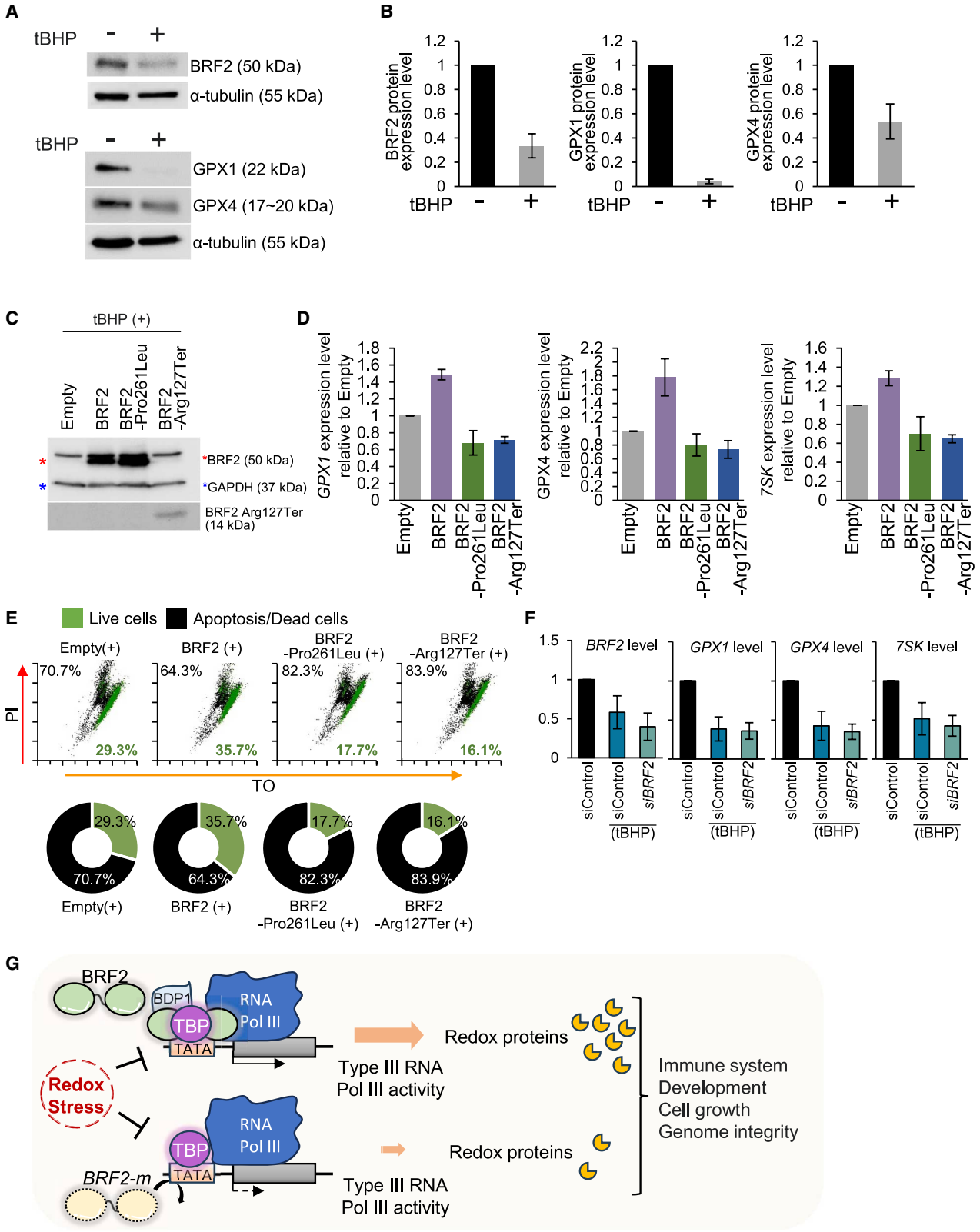

(legend on next page)

Please cite this article in press as: Yoon et al., Biallelic *BRF2* mutations disrupt redox homeostasis as etiological factors in syndromic immunodeficiency and developmental disorders, Molecular Therapy (2025), https://doi.org/10.1016/j.ymthe.2025.08.006

(Figure S13). Collectively, these findings highlight the important role of *BRF2* in supporting cell-cycle progression and maintaining redox homeostasis—critical functions that underpin metabolic processes such as immune response, development, and cellular growth (Figure 7G).

DISCUSSION

Understanding the molecular basis of genetic disorders is critical for elucidating disease mechanisms and informing the development of targeted therapeutic interventions. In this study, we investigate the pathogenic consequences of the biallelic *BRF2* mutations, c.782C>T (p.Pro261Leu) and c.379C>T (p.Arg127Ter), which are associated with impaired RNA Pol III-mediated transcription, particularly affecting the expression of *GPX* family genes. These LoF *BRF2* variants result in heightened sensitivity to redox stress, thereby contributing to the clinical manifestations observed in the patient and suggesting broader implications for syndromic immunodeficiency.

The pathogenicity of the *BRF2* variants is supported by a combination of computational predictions and population-level evidence. Both the nonsense (Arg127Ter) and missense (Pro261Leu) variants exhibited elevated CADD scores (36.0 and 26.7, respectively), consistent with a high likelihood of deleterious impact. Additionally, the Pro261 residue demonstrated strong evolutionary conservation, as reflected by a high phyloP100way score, with proline conserved across amphibians and higher vertebrates (Figure 2B). Notably, neither variant was present in the patient's unaffected sibling, and no homozygous or compound heterozygous individuals harboring these mutations were identified in public variant repositories or our in-house dataset, emphasizing the rarity of these alleles. Structural modeling further revealed that both variants disrupt key interactions within the N-cyclin and C-cyclin repeat domains of BRF2, compromising RNA Pol III functionality. Collectively, these findings support the pathogenicity of the *BRF2* mutations in an autosomal recessive context.

Clinically, the patient's immunological phenotype was atypical, lacking alignment with well-characterized immunodeficiency syndromes. However, the history of severe, recurrent infections—including *Pneumocystis pneumonia*, CMV infection, recurrent bacterial pneumonias, and pneumococcal meningitis—indicated profound immunocompromise. The clinical history of the patient's older sibling, who experienced congenital anomalies and recurrent infections leading to fatal *Pseudomonas* sepsis during infancy, further supports a hereditary immunodeficiency linked to the *BRF2* mutations. These findings suggest a novel immunodeficiency phenotype associated with BRF2 dysfunction that diverges from classical classifications and warrants further investigation.

The single-cell RNA-seq analysis of the patient sample revealed both broad and cell-type-specific transcriptional abnormalities in PBMCs from the patient harboring *BRF2* mutations. Pathways sensitive to intracellular tRNA availability, such as selenocysteine metabolism and the GCN2-mediated amino acid starvation response, were among the most strongly downregulated in the patient sample when compared to controls. This pattern was recapitulated across all major immune cell types, suggesting the systemic impact of BRF2 dysfunction on tRNA-dependent cellular processes. Within this global landscape of immune cells, classical monocytes stood out due to their marked expansion in the patient and the emergence of a distinct subpopulation (m5) largely absent in healthy controls. This cluster was characterized by reduced expression of key selenoprotein genes such as *SELENOK* and *GPX4*, suggesting impaired incorporation of selenocysteine due to defective RNA Pol III-mediated tRNA transcription. In addition, m5 monocytes displayed downregulation of gene modules related to chemotaxis, adhesion, apoptosis regulation, and immune activation, suggesting compromised capacity for immune surveillance and tissue infiltration. These data support the hypothesis that *BRF2* mutations lead to transcriptional insufficiency, affecting both fundamental metabolic processes and monocyte-mediated immune responses, potentially contributing to the patient's immunodeficiency phenotype.

Figure 7. Redox stress and abnormal function of BRF2 cause a defect in type III RNA Pol III-dependent transcription

(A) *BRF2* expression level after treatment with *tert*-butyl hydroperoxide (tBHP). Following the induction of redox stress with tBHP, western blot analysis was performed to confirm *BRF2* expression levels. (B) Quantification of BRF2, GPX1, and GPX4 protein expression levels during redox stress. The expression levels of BRF2 protein under redox stress were quantified using Bio-Rad software. Three independent experiments were performed, and error bars indicate the mean ± SD. (C) Induction of redox stress in HEK293T cells with ectopic expression of *BRF2* or *BRF2* mutants. Protein levels of BRF2 or BRF2 mutants under redox stress were determined via western blot analysis. (D) RNA expression levels of *BRF2*-related genes. Expression levels of *GPX1*, *GPX4*, and *7SK* were confirmed by quantitative real-time PCR in *BRF2*-overexpressing or *BRF2* mutant-overexpressing cells during oxidative stress. Three independent experiments were performed, and error bars indicate the mean ± SD. (E) Cell viability analysis in *BRF2*-overexpressing or *BRF2* mutant-overexpressing HEK293T cells under redox stress. tBHP-induced redox stress was applied to *BRF2*-overexpressing or *BRF2* mutant-overexpressing HEK293T cells. (+) indicates tBHP-treated cells. Cells were stained with propidium iodide (PI) and thiazole orange (TO), and the survival rate was analyzed using FACS. Green dots indicate live cells, while black dots represent apoptotic/dead cells; results were quantified using a FACSCalibur flow cytometer. The ratio of live to apoptotic cells is shown at the bottom, with green indicating the proportion of live cells and black representing apoptotic/dead cells in the doughnut graph. (F) RNA expression levels of *BRF2* and *BRF2*-related genes in *BRF2*-depleted cells under redox stress. HEK293T cells were treated with siControl and si*BRF2*, along with tBHP to induce redox stress, and transcript levels of *BRF2*, *GPX1*, *GPX4*, and *7SK* were measured by quantitative real-time PCR. Three independent experiments were performed, and error bars show the mean ± SD. (G) A proposed model of RNA Pol III-mediated transcription at type III promoters. *BRF2* mutants may impair the ability of the complex to function under redox stress. Normally, TFIIIB, together with *BRF2*, transcribes selenocysteine tRNA, which is crucial for the synthesis of selenoproteins like *GPX1* and *GPX4*. These selenoproteins are vital for maintaining redox homeostasis and protecting cells from oxidative damage. However, under oxidative stress, *BRF2* mutants may fail to effectively form the TFIIIB complex, leading to reduced expression of selenocysteine tRNA and, subsequently, lower selenoprotein production. This deficiency may result in significant disruptions to essential cellular processes, including immune response, development, cell growth, and genome stability.

Please cite this article in press as: Yoon et al., Biallelic *BRF2* mutations disrupt redox homeostasis as etiological factors in syndromic immunodeficiency and developmental disorders, Molecular Therapy (2025), https://doi.org/10.1016/j.ymthe.2025.08.006

At the molecular level, this study demonstrates that biallelic *BRF2* mutations disrupt RNA Pol III activity specifically at type III promoters, leading to transcriptional dysregulation of critical noncoding RNAs. RNA Pol III is essential for the synthesis of small structural RNAs, such as tRNAs and spliceosomal RNAs, which are vital for protein translation and RNA processing. Consequently, impairment of RNA Pol III transcription resulting from *BRF2* mutations is expected to compromise fundamental aspects of cellular homeostasis. Notably, beyond canonical RNA Pol III targets, we identified a selective downregulation of redox-associated genes, including *GPX1* and *GPX4*, as well as U6 spliceosomal RNA. These findings highlight a mechanistic link between *BRF2*-dependent RNA Pol III transcription and the regulation of redox homeostasis, which plays a critical role in immune cell development and function.[6,22]

Notably, impaired expression of essential selenoproteins, including GPX4, a key enzyme responsible for detoxifying ROS was observed, implicating *BRF2* mutations in the disruption of redox-sensitive pathways. The transcription of SeCys tRNA, which is required for the synthesis of antioxidant enzymes such as GPX1 and GPX4, is mediated by RNA Pol III, with *BRF2* playing a central regulatory role. Dysregulation of *GPX1* and *GPX4* expression suggests that redox imbalance may significantly contribute to the patient's clinical phenotype.[32–35] Redox homeostasis, maintained through a dynamic equilibrium between oxidants and antioxidants, is essential for cellular viability and physiological function.[36] Glutathione peroxidases are critical for ROS detoxification and cellular protection against oxidative injury.[12] Dysfunction of these enzymes may shift the cellular redox state toward oxidative stress, thereby initiating downstream events that drive disease pathogenesis.[37] Under moderate oxidative stress, BRF2 activity is rapidly suppressed via redox-dependent modifications, functioning as a regulatory mechanism to limit SeCys tRNA synthesis. This early downregulation might reflect a cellular strategy to conserve resources and prioritize Nrf2-driven stress-response gene expression.[2] During this initial phase, the existing SeCys tRNA pool is sufficient to support basal selenoprotein synthesis. However, under prolonged oxidative stress, this suppression becomes detrimental. To meet the increased demand for SeCys tRNAs, BRF2 must be reactivated or overexpressed, enabling continued selenoprotein expression. This adaptive BRF2 upregulation appears context dependent, allowing cells in persistently stressed environments to maintain redox homeostasis and evade apoptosis.

A growing body of literature implicates redox imbalance in a broad array of human diseases, including neurodegenerative conditions, malignancies, and developmental disorders.[14–16] In this context, *BRF2* depletion was associated with delayed cell growth, potentially attributable to redox dysregulation impacting cell-cycle progression or DNA damage repair. Moreover, oxidative stress has been shown to perturb intracellular signaling, impair cell proliferation and differentiation, and promote genomic instability, processes that are closely linked to the etiology of developmental abnormalities.[38] ROS serve as key modulators of diverse biological processes, including apoptosis, cell proliferation, lineage commitment, and intracellular signaling cascades.[39] During embryogenesis, ROS act as signaling intermediates, influencing TFs involved in immune cell development, blastocyst maturation, neurogenesis, and limb morphogenesis.[39–42] Accordingly, perturbations in redox balance can exert profound effects on normal development. Oxidative modifications to DNA further contribute to genomic instability and have been implicated in cancer pathogenesis.[43,44] There is increasing evidence that oxidative stress during the prenatal period can result in craniofacial anomalies and neurodevelopmental conditions such as autism spectrum disorder and attention-deficit/hyperactivity disorder.[45–47] Thus, the maintenance of redox equilibrium is fundamental to ensuring cellular integrity and proper organogenesis.

In murine models, homozygous loss of *GPX4* results in embryonic lethality by embryonic day 7.5, whereas heterozygous deficiency confers increased vulnerability to oxidative stress.[48–51] Furthermore, *GPX4* depletion induces cell death in critical tissues, including the brain, liver, and heart, culminating in a spectrum of developmental anomalies.[52,53] Deficiency in *GPX4* has also been implicated in motor neuron degeneration, paralysis, and impaired T cell-mediated immune responses.[52–54] Clinically, mutations in *GPX4* are causative of Sedaghatian-type spondylometaphyseal dysplasia, a rare and lethal autosomal recessive disorder characterized by skeletal malformations, agenesis or hypoplasia of the corpus callosum and cerebellum, and profound developmental delays.[52,55–57] These phenotypes exhibit striking similarities to the congenital anomalies observed in our patient, including polydactyly, craniofacial dysmorphism, immunodeficiency, and increased susceptibility to infection. These findings emphasize that redox imbalance, particularly due to impaired glutathione peroxidase activity, can precipitate severe prenatal developmental abnormalities and immunological dysfunction.

Restoration of redox equilibrium, whether through antioxidant supplementation or modulation of redox-regulatory pathways, may represent a viable strategy to attenuate disease progression and improve clinical outcomes.[58] Our data indicate that elucidating the molecular mechanisms underlying redox dysregulation, particularly in the context of *BRF2* mutations, is essential for the development of targeted therapeutic interventions. Accordingly, we propose that correcting redox imbalance may provide a promising approach for managing *BRF2*-associated immunodeficiency and developmental delay. Therapeutic strategies aimed at restoring *BRF2*-dependent redox homeostasis may mitigate disease severity and alleviate clinical symptoms.[59,60] Moreover, the identification of downstream effectors in redox signaling pathways could reveal additional pharmacological targets. Notably, our study demonstrated that selenium supplementation rescued the impaired *GPX4* expression and redox stress responses in *BRF2*-mutant cells, suggesting that selenium may partially restore compromised antioxidant defenses arising from *BRF2* dysfunction.

This study is not without limitations. The primary limitation lies in its reliance on data derived from a single patient, which inherently

Please cite this article in press as: Yoon et al., Biallelic *BRF2* mutations disrupt redox homeostasis as etiological factors in syndromic immunodeficiency and developmental disorders, Molecular Therapy (2025), https://doi.org/10.1016/j.ymthe.2025.08.006

constrains the generalizability of the findings. Nevertheless, the integration of clinical observations, genetic analyses, and functional assays provides robust evidence implicating *BRF2* LoF mutations in the observed clinical phenotypes. The identification of biallelic *BRF2* mutations resulting in impaired RNA Pol III function—particularly at type III promoters—establishes a molecular framework for subclassifying patients based on their underlying genetic etiology. To assess the broader relevance of these findings, we analyzed genomic data from roughly 7,500 exomes and 5,000 genomes of rare disease patients and their family members but did not identify any additional cases with biallelic *BRF2* mutations (data not shown). This suggests that such mutations represent an exceptionally rare genetic event, even within the Korean population. The complexity of disorders associated with *BRF2* mutations underscores the necessity of a multidisciplinary investigative approach, integrating genomics, cellular biology, and clinical insights to fully elucidate disease mechanisms.[61–63] The application of diverse experimental strategies—including molecular assays, advanced imaging, and *in vivo* modeling—will be essential for further clarifying pathogenesis and identifying actionable therapeutic targets.[64–67] This study delineates the molecular underpinnings of the multisystem anomalies and hemato-immunologic abnormalities associated with *BRF2* mutations that compromise RNA Pol III activity. We underscore the central role of redox imbalance in disease pathogenesis and propose that targeted interventions aimed at restoring redox homeostasis may offer clinical benefit. Our ongoing work focuses on dissecting the complexity of redox signaling networks and defining how *BRF2*-mediated transcriptional programs modulate these pathways, with the goal of informing precision medicine strategies tailored to the genetic profiles of affected individuals.

MATERIALS AND METHODS

Whole-exome and whole-genome sequencing for pathogenic variant identification

Whole-exome sequencing of the proband and their parents was conducted as a trio using Illumina technology, following previously described methodologies.[68] Sequence reads were aligned to the human reference genome (GRCh37) and processed in accordance with the Genome Analysis Toolkit Best Practices workflow.[69] Variant annotation was conducted using ANNOVAR with reference to the RefSeq gene set and gnomAD.[25,70] The ClinVar database was additionally consulted to identify any previously reported variants in the proband.[71] To identify novel pathogenic variants, the analysis focused on rare, non-silent variants, including nonsynonymous SNVs, coding insertions or deletions, and splicing variants, with an allele frequency of less than 0.001 in gnomAD. Parental exome data were used to identify *de novo* variants as well as homozygous or compound heterozygous variants, based on dominant and recessive inheritance models, respectively. Candidate variants were classified according to the guidelines of the American College of Medical Genetics and Genomics.[72]

Following the identification of biallelic *BRF2* variants by whole-exome sequencing, whole-genome sequencing was subsequently conducted on the proband to screen for additional pathogenic variants, including those in noncoding or structural regions. Sequence reads were generated using the Illumina NovaSeq 6000 platform and processed as described above, except that the GRCh38 human reference genome was used. Details of the variant calling and filtration pipeline specific to whole-genome sequencing have been described previously.[73]

Cell culture and induction of redox stress

HEK293T cells were cultured in Dulbecco's modified Eagle's medium (catalog no. 11995-073, Gibco, USA) supplemented with 10% fetal bovine serum (FBS; catalog no. 16000-044, Gibco) and 100 U/mL penicillin-streptomycin (catalog no. 15140-122, Gibco). Cells were maintained in a humidified incubator with 5% CO_2. To induce redox stress, cells were treated with 600 μM tBHP (catalog no. 458139, Sigma-Aldrich, USA) for 3 h.

Depletion and expression of *BRF2*

BRF2 knockdown was achieved using siRNAs specific to human *BRF2* (siRNA ID: 55290) and a negative control (catalog no. SN-1003), both predesigned and synthesized by Bioneer (Republic of Korea). siRNAs were diluted in Opti-MEM medium (catalog no. 31985-070, Gibco) and transfected using Lipofectamine RNAiMAX (catalog no. INV-13778-150, Thermo Fisher, USA). HEK293T cells were incubated with the transfection complex for 48 h under standard culture conditions. The sequence of the siRNA targeting *BRF2* was 5′-GAGAA GATGCTGTCTCGAA-3′. To overexpress *BRF2*, HEK293T cells were transfected with the pCMV-SPORT6-*BRF2* vector obtained from the Korea Human Gene Bank (Republic of Korea; clone ID: hMU000733). Two mutant constructs were generated: a cytosine-to-thymine substitution at nucleotide position 782 (Pro261Leu) and a cytosine-to-thymine substitution at position 379 (Arg127Ter). All expression vectors, including the wild-type and mutant forms, were validated by DNA sequencing prior to use.

Quantitative real-time PCR

Total RNA was extracted using the RNeasy Mini Kit (catalog no. 74104, Qiagen, Germany), and cDNA synthesis was performed using the cDNA Synthesis Kit (catalog no. EZ005, Enzynomics, Republic of Korea), following the manufacturer's instructions. Quantitative real-time PCR was carried out using SYBR Green (catalog no. K-6251, Bioneer) on a CFX Connect Real-Time PCR system (catalog no. 1855201, Bio-Rad, USA). The primer sequences used for qRT-PCR were as follows: *BRF2* (forward primer: 5′-cagaagtggagacccgagag-3′, reverse primer: 5′-cagggagggttagggacact-3′),[74] *7SK* (forward primer: 5′-attgatcgccagggttgat-3′, reverse primer: 5′-ctctatcggg gatggtcgt-3′),[75] *GPX1* (forward primer: 5′-tgctcggcttcccgtgcaaccagt-3′, reverse primer 5′-ggtgatgagcttggggtcggtcat-3′),[76] *GPX4* (forward primer: 5′-gaggcaagaccgaagtaaactac-3′, reverse primer: 5′-ccgaac tggttacacgggaa-3′),[77] and *5s rRNA* (forward primer: 5′-ggccatac caccctgaacgc -3′, reverse primer: 5′-cagcacccggtattcccagg -3′).[2] Each quantitative real-time PCR reaction included 10 ng cDNA. The thermal cycling protocol consisted of an initial denaturation at 95°C for 3 min, followed by 40 cycles of 95°C for 10 s, 53°C for

Please cite this article in press as: Yoon et al., Biallelic *BRF2* mutations disrupt redox homeostasis as etiological factors in syndromic immunodeficiency and developmental disorders, Molecular Therapy (2025), https://doi.org/10.1016/j.ymthe.2025.08.006

10 s, and 72°C for 30 s. Relative expression levels were calculated using the $2^{-\Delta\Delta Cq}$ method, with *5s rRNA* serving as the endogenous control (ΔCq = Cq_target − Cq_control; ΔΔCq = ΔCq_experimental − ΔCq_baseline).

Bulk RNA-seq for *BRF2*-depleted cell lines

Total RNA was extracted from si*BRF2*-treated cells using the RNeasy Mini Kit (catalog no. 74104, Qiagen). RNA integrity was assessed using the Agilent 2100 Bioanalyzer (Agilent Technologies, USA). Libraries were prepared with the TruSeq Stranded Total RNA Ribo-Zero H/M/R kit (Illumina, USA), and sequencing was performed on the Illumina HiSeq X platform. Reads were aligned to the human reference genome (GRCh38) using STAR in 2-pass mode.[78] Transcript and gene expression levels were quantified using RSEM.[79] DEGs were identified using DESeq2,[80] with statistical thresholds of adjusted $p < 0.001$ and absolute $\log_2$ fold change >0.5. Principal-component analysis (PCA) was conducted using the 500 most variable genes. Heatmaps of selected gene sets were generated using the *pheatmap* package.[81] GSEA was performed using the Enrichr database.[82]

Western blot analysis

Western blotting was performed as described previously.[83] Cells were washed with PBS and lysed using cell lysis buffer supplemented with protease inhibitor cocktail (catalog no. 1873580, Roche, Switzerland) and 1 mM PMSF. The primary antibodies used were as follows: anti-BRF2 (catalog no. sc-390312, Santa Cruz Biotechnology, USA), anti-GPX1 (catalog no. ab108429, Abcam, UK), anti-GPX4 (catalog no. ab125066, Abcam), and anti-glyceraldehyde 3-phosphate dehydrogenase (catalog no. ab8245, Abcam). The secondary antibodies included horseradish peroxidase (HRP)-conjugated anti-mouse IgG (catalog no. 115-035-003, Jackson ImmunoResearch Laboratories, USA) and HRP-conjugated anti-rabbit IgG (catalog no. 111-035-003, Jackson ImmunoResearch Laboratories). Western blot signals were developed with the ChemiDoc MP Imaging System (catalog no. BR17001402, Bio-Rad, USA). Protein expression was quantified using BioRad Image Lab software.

Cell viability assay

Cell viability was assessed using a cell viability kit (catalog no. 349483, BD Biosciences, USA) in accordance with the manufacturer's instructions. Cells were stained with thiazole orange and propidium iodide, followed by a 5-min incubation. The survival rate was determined by FACS analysis using a BD Accuri C6 cytometer, with data acquisition and analysis conducted using Accuri C6 software.

Cell-cycle analysis

Cells were harvested and fixed in 70% ethanol overnight. After ethanol removal, cells were stained with propidium iodide. Cell-cycle progression was analyzed using a FACSCalibur flow cytometer (BD Biosciences) and quantified with ModFit software.

PBMC isolation

PBMCs were isolated from 16 mL of blood obtained from the patient using heparin-coated CPT tubes (BD Biosciences). Following collection, samples were centrifuged at 1,800 × *g* for 20 min to separate the cell layers. The PBMC layer was carefully harvested and transferred into a 15-mL conical tube containing 1 mL RPMI medium supplemented with 10% FBS. Purified PBMCs were cryopreserved in Cell Banker 1 (AMSBIO, UK) as the cryoprotectant medium and stored in liquid nitrogen until single-cell RNA library preparation. All procedures were approved by the SNUH institutional review board (IRB nos. 2204-112-1317 and 1101-110-353), and informed consent was obtained from the study participant and her legal guardians.

Single-cell cDNA and library preparation

Single-cell cDNA synthesis and library preparation were performed according to the manufacturer's protocols (10x Genomics [USA], 5′ HT v2, CG000424, Rev D). To enable multiplexed sample analysis, samples were pooled into a single Gel Beads-in-Emulsion (GEM) reaction. GEMs were generated using the Chromium Controller (10x Genomics), where individual cells were encapsulated with gel beads containing 10x barcodes, unique molecular identifiers, and oligo(dT) primers. Reverse transcription was initiated immediately following GEM formation to convert mRNA transcripts into cDNA. After disassembly of the GEMs, full-length cDNAs tagged with 10x barcodes were purified using SILANE magnetic beads (catalog no. PN 2000048, 10x Genomics) and amplified to achieve sufficient yield. Amplified cDNAs were then used to construct gene expression libraries, incorporating P5 and P7 priming sites for compatibility with the NovaSeq sequencing platform (Illumina, USA). Library quality and yield were assessed using the 4150 TapeStation system (Agilent Technologies).

Genomic DNA purification and single-nucleotide polymorphism array

Genomic DNA (gDNA) was extracted from PBMC samples using the QIAamp DNA Kit (Qiagen). The extraction process employed a rapid spin-column method utilizing optimized buffers and enzymes to lyse PBMCs and stabilize nucleic acids. Following lysis, multiple wash steps were carried out via the spin column to eliminate contaminants, and the purified gDNA was eluted in Buffer AE. The quality of the isolated gDNA was assessed by measuring the concentration and purity of double-stranded DNA using a NanoDrop spectrophotometer. Additional quality control was performed using the TapeStation 4200 system. The gDNA samples were then analyzed for single-nucleotide polymorphisms using the Illumina Infinium Asian Screening Array on a bead chip platform.

Single-cell RNA-seq quality control and data analysis

The generated FASTQ files were aligned to the human reference transcriptome (hg38) using Cell Ranger (version 7.1.0). Samples were demultiplexed using Demuxafy[84] to assign each cell to its originating donor. To reduce ambient RNA contamination, SoupX was applied, and doublets were identified and removed using scDblFinder. Quality control was performed using the Seurat package (version 5.0.3), excluding cells with fewer than 200 or more than 3,000 detected genes, as well as those with mitochondrial gene content exceeding 5% or hemoglobin contamination exceeding

10%. After filtering, a total of 42,735 cells were retained from the patient and 4 age-matched pediatric healthy controls. All samples were merged into a single Seurat object for data integration and normalization, using default parameters. The top 2,000 variable features were selected for PCA. Harmony was employed to correct for potential batch effects, and dimensionality reduction was further refined using uniform manifold approximation and projection. Clustering was conducted using the Louvain algorithm, and clusters were manually annotated based on canonical immune cell markers. DEGs were identified via the Wilcoxon rank-sum test, with significance defined as $p < 0.05$. GSEA was performed on the DEGs using the fgsea package, and results were visualized with R and GraphPad Prism (version 8).

DATA AVAILABILITY

The datasets generated and/or analyzed during the present study are available in the National Center for Biotechnology Information (NCBI) repository: https://www.ncbi.nlm.nih.gov/geo/query/acc.cgi?acc=GSE280147 and https://www.ncbi.nlm.nih.gov/geo/query/acc.cgi?acc=GSE280098.

ACKNOWLEDGMENTS

We would like to express our sincere gratitude to our patient and her family, who generously provided their blood samples for this study. Their willingness to participate has been essential to advancing our research into the underlying causes of this rare disease. We also appreciate the invaluable support of the medical professionals and researchers who contributed to the collection and analysis of clinical data, helping to deepen our understanding of this condition. This research was supported by National Research Foundation of Korea grants funded by the Korean government (MSIT) (RS-2023-00208191 and 2022M3A9J4079468) and the Kun-hee Lee Seoul National University Hospital Child Cancer & Rare Disease Project, Republic of Korea (25B-001-0500).

AUTHOR CONTRIBUTIONS

S.Y., S.L., H.K., H.-S.K., J.H.J., S.H., S.Y.K., S. Jang, H.L., H.S.C., A.C., S. Jeong, C.S.-Y.J., E.-H.C., K.A., H.J.K., K.P.K., and J.-H.C. designed and structured the experiments. S.Y., S.L., and H.K. performed the experiments. S.Y., S.L., H.K., H.-S.K., K.P.K., and J.-H.C. analyzed the data and wrote the manuscript. All authors gave final approval of the manuscript.

DECLARATION OF INTERESTS

The authors declare no competing interests.

SUPPLEMENTAL INFORMATION

Supplemental information can be found online at https://doi.org/10.1016/j.ymthe.2025.08.006.

REFERENCES

1. Macneil, L.T., and Walhout, A.J.M. (2011). Gene regulatory networks and the role of robustness and stochasticity in the control of gene expression. Genome Res. *21*, 645–657.
2. Gouge, J., Satia, K., Guthertz, N., Widya, M., Thompson, A.J., Cousin, P., Dergai, O., Hernandez, N., and Vannini, A. (2015). Redox Signaling by the RNA Polymerase III TFIIB-Related Factor Brf2. Cell *163*, 1375–1387.
3. Kassavetis, G.A., Letts, G.A., and Geiduschek, E.P. (1999). A minimal RNA polymerase III transcription system. EMBO J. *18*, 5042–5051.
4. Schramm, L., and Hernandez, N. (2002). Recruitment of RNA polymerase III to its target promoters. Genes Dev. *16*, 2593–2620.
5. Kim, H.K., Yeom, J.-H., and Kay, M.A. (2020). Transfer RNA-Derived Small RNAs: Another Layer of Gene Regulation and Novel Targets for Disease Therapeutics. Mol. Ther. *28*, 2340–2357.
6. Willis, I.M., and Moir, R.D. (2018). Signaling to and from the RNA Polymerase III Transcription and Processing Machinery. Annu. Rev. Biochem. *87*, 75–100.
7. Han, Y., Yan, C., Fishbain, S., Ivanov, I., and He, Y. (2018). Structural visualization of RNA polymerase III transcription machineries. Cell Discov. *4*, 40.
8. Ng, C.K.Y., Martelotto, L.G., Gauthier, A., Wen, H.-C., Piscuoglio, S., Lim, R.S., Cowell, C.F., Wilkerson, P.M., Wai, P., Rodrigues, D.N., et al. (2015). Intra-tumor genetic heterogeneity and alternative driver genetic alterations in breast cancers with heterogeneous HER2 gene amplification. Genome Biol. *16*, 107.
9. Cabarcas, S., and Schramm, L. (2011). RNA polymerase III transcription in cancer: the BRF2 connection. Mol. Cancer *10*, 47.
10. Borck, G., Hög, F., Dentici, M.L., Tan, P.L., Sowada, N., Medeira, A., Gueneau, L., Thiele, H., Kousi, M., Lepri, F., et al. (2015). BRF1 mutations alter RNA polymerase III-dependent transcription and cause neurodevelopmental anomalies. Genome Res. *25*, 155–166.
11. Yeganeh, M., and Hernandez, N. (2020). RNA polymerase III transcription as a disease factor. Genes Dev. *34*, 865–882.
12. Pei, J., Pan, X., Wei, G., and Hua, Y. (2023). Research progress of glutathione peroxidase family (GPX) in redoxidation. Front. Pharmacol. *14*, 1147414.
13. Kasaikina, M.V., Hatfield, D.L., and Gladyshev, V.N. (2012). Understanding selenoprotein function and regulation through the use of rodent models. Biochim. Biophys. Acta *1823*, 1633–1642.
14. Cobb, C.A., and Cole, M.P. (2015). Oxidative and nitrative stress in neurodegeneration. Neurobiol. Dis. *84*, 4–21.
15. Pervaiz, S., Bellot, G.L., Lemoine, A., and Brenner, C. (2020). Redox signaling in the pathogenesis of human disease and the regulatory role of autophagy. Int. Rev. Cell Mol. Biol. *352*, 189–214.
16. Hansen, J.M., Jones, D.P., and Harris, C. (2020). The Redox Theory of Development. Antioxid. Redox Signal. *32*, 715–740.
17. Ballow, M., Sánchez-Ramón, S., and Walter, J.E. (2022). Secondary Immune Deficiency and Primary Immune Deficiency Crossovers: Hematological Malignancies and Autoimmune Diseases. Front. Immunol. *13*, 928062.
18. Mayor, P.C., Eng, K.H., Singel, K.L., Abrams, S.I., Odunsi, K., Moysich, K.B., Fuleihan, R., Garabedian, E., Lugar, P., Ochs, H.D., et al. (2018). Cancer in primary immunodeficiency diseases: Cancer incidence in the United States Immune Deficiency Network Registry. J. Allergy Clin. Immunol. *141*, 1028–1035.
19. Amaya-Uribe, L., Rojas, M., Azizi, G., Anaya, J.M., and Gershwin, M.E. (2019). Primary immunodeficiency and autoimmunity: A comprehensive review. J. Autoimmun. *99*, 52–72.
20. Wilkie, A.O.M. (2021). Genetics of craniofacial anomalies. In Oxford Textbook of Plastic and Reconstructive Surgery, H. Nishikawa, F.V. Mehendale, D.C.G. Sainsbury, S. Kay, D. McCombe, and D. Wilks, eds. (Oxford University Press), pp. 101290.
21. Lee, Y. (2011). The Relationships among Language, Communicative Abilities and Motor, Cognitive, and Socio-Emotional Development in Toddlers with Language Delays. Commun. Sci. Disord. *16*, 1–12.
22. Lata, E., Choquet, K., Sagliocco, F., Brais, B., Bernard, G., and Teichmann, M. (2021). RNA Polymerase III Subunit Mutations in Genetic Diseases. Front. Mol. Biosci. *8*, 696438.
23. Schubach, M., Maass, T., Nazaretyan, L., Röner, S., and Kircher, M. (2024). CADD v1.7: using protein language models, regulatory CNNs and other nucleotide-level scores to improve genome-wide variant predictions. Nucleic Acids Res. *52*, D1143–D1154.
24. Yoon, J.G., Lee, S., Cho, J., Kim, N., Kim, S., Kim, M.J., Kim, S.Y., Moon, J., and Chae, J.H. (2024). Diagnostic uplift through the implementation of short tandem repeat analysis using exome sequencing. Eur. J. Hum. Genet. *32*, 584–587.
25. Karczewski, K.J., Francioli, L.C., Tiao, G., Cummings, B.B., Alföldi, J., Wang, Q., Collins, R.L., Laricchia, K.M., Ganna, A., Birnbaum, D.P., et al. (2020). The mutational constraint spectrum quantified from variation in 141,456 humans. Nature *581*, 434–443.
26. Lagrange, T., Kapanidis, A.N., Tang, H., Reinberg, D., and Ebright, R.H. (1998). New core promoter element in RNA polymerase II-dependent transcription: sequence-specific DNA binding by transcription factor IIB. Genes Dev. *12*, 34–44.

27. Tsai, F.T., and Sigler, P.B. (2000). Structural basis of preinitiation complex assembly on human Pol II promoters. EMBO J. *19*, 25–36.

28. Arimbasseri, A.G., Rijal, K., and Maraia, R.J. (2014). Comparative overview of RNA polymerase II and III transcription cycles, with focus on RNA polymerase III termination and reinitiation. Transcription *5*, e27639.

29. Nagai, M.A. (2016). Pleckstrin homology-like domain, family A, member 1 (PHLDA1) and cancer. Biomed. Rep. *4*, 275–281.

30. Mesquita, G., Silva, T., Gomes, A.C., Oliveira, P.F., Alves, M.G., Fernandes, R., Almeida, A.A., Moreira, A.C., and Gomes, M.S. (2020). H-Ferritin is essential for macrophages' capacity to store or detoxify exogenously added iron. Sci. Rep. *10*, 3061.

31. Vannini, A., and Cramer, P. (2012). Conservation between the RNA Polymerase I, II, and III Transcription Initiation Machineries. Mol. Cell *45*, 439–446.

32. Lubos, E., Loscalzo, J., and Handy, D.E. (2011). Glutathione peroxidase-1 in health and disease: from molecular mechanisms to therapeutic opportunities. Antioxid. Redox Signal. *15*, 1957–1997.

33. Weaver, K., and Skouta, R. (2022). The Selenoprotein Glutathione Peroxidase 4: From Molecular Mechanisms to Novel Therapeutic Opportunities. Biomedicines *10*, 891.

34. Li, C., Deng, X., Zhang, W., Xie, X., Conrad, M., Liu, Y., Angeli, J.P.F., and Lai, L. (2019). Novel Allosteric Activators for Ferroptosis Regulator Glutathione Peroxidase 4. J. Med. Chem. *62*, 266–275.

35. Handy, D.E., and Loscalzo, J. (2022). The role of glutathione peroxidase-1 in health and disease. Free Radic. Biol. Med. *188*, 146–161.

36. Li, Y., Zhang, X., Wang, Z., Li, B., and Zhu, H. (2023). Modulation of redox homeostasis: A strategy to overcome cancer drug resistance. Front. Pharmacol. *14*, 1156538.

37. Heitzer, T., Schlinzig, T., Krohn, K., Meinertz, T., and Münzel, T. (2001). Endothelial dysfunction, oxidative stress, and risk of cardiovascular events in patients with coronary artery disease. Circulation *104*, 2673–2678.

38. Liu, Y., Shi, Y., Han, R., Liu, C., Qin, X., Li, P., and Gu, R. (2023). Signaling pathways of oxidative stress response: the potential therapeutic targets in gastric cancer. Front. Immunol. *14*, 1139589.

39. Dennery, P.A. (2007). Effects of oxidative stress on embryonic development. Birth Defects Res. C Embryo Today *81*, 155–162.

40. Liu, W., Peng, J., Wu, Y., Ye, Z., Zong, Z., Wu, R., and Li, H. (2023). Immune and inflammatory mechanisms and therapeutic targets of gout: An update. Int. Immunopharmacol. *121*, 110466.

41. Ford, K., Hanley, C.J., Mellone, M., Szyndralewiez, C., Heitz, F., Wiesel, P., Wood, O., Machado, M., Lopez, M.A., Ganesan, A.P., et al. (2020). NOX4 Inhibition Potentiates Immunotherapy by Overcoming Cancer-Associated Fibroblast-Mediated CD8 T-cell Exclusion from Tumors. Cancer Res. *80*, 1846–1860.

42. Sies, H., and Jones, D.P. (2020). Reactive oxygen species (ROS) as pleiotropic physiological signalling agents. Nat. Rev. Mol. Cell Biol. *21*, 363–383.

43. Poulsen, H.E. (2005). Oxidative DNA modifications. Exp. Toxicol. Pathol. *57*, 161–169.

44. Ufer, C., and Wang, C.C. (2011). The roles of glutathione peroxidases during embryo development. Front. Mol. Neurosci. *4*, 12.

45. Carmichael, S.L., Yang, W., Ma, C., Desrosiers, T.A., Weber, K., Collins, R.T., Nestoridi, E., and Shaw, G.M.; National Birth Defects Prevention Study (2023). Oxidative balance scores and neural crest cell-related congenital anomalies. Birth Defects Res. *115*, 1151–1162.

46. Divvela, S.S.K., Gallorini, M., Gellisch, M., Patel, G.D., Saso, L., and Brand-Saberi, B. (2025). Navigating redox imbalance: the role of oxidative stress in embryonic development and long-term health outcomes. Front. Cell Dev. Biol. *13*, 1521336.

47. Pham, C., Thomson, S., Chin, S.-T., Vuillermin, P., O'Hely, M., Burgner, D., Tanner, S., Saffery, R., Mansell, T., Bong, S., et al. (2023). Maternal oxidative stress during pregnancy associated with emotional and behavioural problems in early childhood: implications for foetal programming. Mol. Psychiatry *28*, 3760–3768.

48. Imai, H., Hirao, F., Sakamoto, T., Sekine, K., Mizukura, Y., Saito, M., Kitamoto, T., Hayasaka, M., Hanaoka, K., and Nakagawa, Y. (2003). Early embryonic lethality caused by targeted disruption of the mouse PHGPx gene. Biochem. Biophys. Res. Commun. *305*, 278–286.

49. Ran, Q., Van Remmen, H., Gu, M., Qi, W., Roberts, L.J., Prolla, T., and Richardson, A. (2003). Embryonic fibroblasts from Gpx4+/− mice: a novel model for studying the role of membrane peroxidation in biological processes. Free Radic. Biol. Med. *35*, 1101–1109.

50. Xie, Y., Kang, R., Klionsky, D.J., and Tang, D. (2023). GPX4 in cell death, autophagy, and disease. Autophagy *19*, 2621–2638.

51. Yant, L.J., Ran, Q., Rao, L., Van Remmen, H., Shibatani, T., Belter, J.G., Motta, L., Richardson, A., and Prolla, T.A. (2003). The selenoprotein GPX4 is essential for mouse development and protects from radiation and oxidative damage insults. Free Radic. Biol. Med. *34*, 496–502.

52. Cheff, D.M., Muotri, A.R., Stockwell, B.R., Schmidt, E.E., Ran, Q., Kartha, R.V., Johnson, S.C., Mittal, P., Arnér, E.S.J., Wigby, K.M., et al. (2021). Development of therapies for rare genetic disorders of GPX4: roadmap and opportunities. Orphanet J. Rare Dis. *16*, 446.

53. Imai, H., Matsuoka, M., Kumagai, T., Sakamoto, T., and Koumura, T. (2017). Lipid Peroxidation-Dependent Cell Death Regulated by GPx4 and Ferroptosis. Curr. Top. Microbiol. Immunol. *403*, 143–170.

54. Chen, H., Chomyn, A., and Chan, D.C. (2005). Disruption of fusion results in mitochondrial heterogeneity and dysfunction. J. Biol. Chem. *280*, 26185–26192.

55. Hambright, W.S., Fonseca, R.S., Chen, L., Na, R., and Ran, Q. (2017). Ablation of ferroptosis regulator glutathione peroxidase 4 in forebrain neurons promotes cognitive impairment and neurodegeneration. Redox Biol. *12*, 8–17.

56. Fedida, A., Ben Harouch, S., Kalfon, L., Abunassar, Z., Omari, H., Mandel, H., and Falik-Zaccai, T.C. (2020). Sedaghatian-type spondylometaphyseal dysplasia: Whole exome sequencing in neonatal dry blood spots enabled identification of a novel variant in GPX4. Eur. J. Med. Genet. *63*, 104020.

57. Zhang, W., Liu, Y., Liao, Y., Zhu, C., and Zou, Z. (2024). GPX4, ferroptosis, and diseases. Biomed. Pharmacother. *174*, 116512.

58. Allemann, M.S., Lee, P., Beer, J.H., and Saeedi Saravi, S.S. (2023). Targeting the redox system for cardiovascular regeneration in aging. Aging Cell *22*, e14020.

59. Shi, Z., Li, X., Chen, J., Dai, Z., Zhu, Y., Wu, T., Liu, Q., Qin, H., Zhang, Y., and Chen, H. (2024). Enzyme-like biomimetic oral-agent enabling modulating gut microbiota and restoring redox homeostasis to treat inflammatory bowel disease. Bioact. Mater. *35*, 167–180.

60. Han, P., Cai, Y., Wang, Y., Weng, W., Chen, Y., Wang, M., Zhan, H., Yu, X., Wang, T., Shao, M., and Sun, H. (2021). Artemether ameliorates kidney injury by restoring redox imbalance and improving mitochondrial function in Adriamycin nephropathy in mice. Sci. Rep. *11*, 1266.

61. Brown, H.L., Sherburn, I.A., Gaff, C., Taylor, N., and Best, S. (2022). Structured approaches to implementation of clinical genomics: A scoping review. Genet. Med. *24*, 1415–1424.

62. Ardizzone, A., Capra, A.P., Campolo, M., Filippone, A., Esposito, E., and Briuglia, S. (2022). Neurofibromatosis: New Clinical Challenges in the Era of COVID-19. Biomedicines *10*, 940.

63. Merker, V.L., Slobogean, B., Jordan, J.T., Langmead, S., Meterko, M., Charns, M.P., Elwy, A.R., Blakeley, J.O., and Plotkin, S.R. (2022). Understanding barriers to diagnosis in a rare, genetic disease: Delays and errors in diagnosing schwannomatosis. Am. J. Med. Genet. A. *188*, 2672–2683.

64. Yoon, S., Choi, E.-H., Kim, J.-W., and Kim, K.P. (2018). Structured illumination microscopy imaging reveals localization of replication protein A between chromosome lateral elements during mammalian meiosis. Exp. Mol. Med. *50*, 1–12.

65. Choi, E.H., Yoon, S., Hahn, Y., and Kim, K.P. (2017). Cellular Dynamics of Rad51 and Rad54 in Response to Postreplicative Stress and DNA Damage in HeLa Cells. Mol. Cells *40*, 143–150.

66. Choi, E.H., and Kim, K.P. (2019). E2F1 facilitates DNA break repair by localizing to break sites and enhancing the expression of homologous recombination factors. Exp. Mol. Med. *51*, 1–12.

67. Yoon, S., Lee, B.-K., and Kim, K.P. (2023). Caffeine enhances chemosensitivity to irinotecan in the treatment of colorectal cancer. Phytomedicine. *121*, 155120.

68. Lee, S., Eum, J., Park, S., Ki, S., Hwang, B.J., Kee, Y., and Chae, J.H. (2022). TNNT1 myopathy with novel compound heterozygous mutations. Neuromuscul. Disord. *32*, 176–184.

69. McKenna, A., Hanna, M., Banks, E., Sivachenko, A., Cibulskis, K., Kernytsky, A., Garimella, K., Altshuler, D., Gabriel, S., Daly, M., and DePristo, M.A. (2010). The Genome Analysis Toolkit: a MapReduce framework for analyzing next-generation DNA sequencing data. Genome Res. *20*, 1297–1303.

70. Wang, K., Li, M., and Hakonarson, H. (2010). ANNOVAR: functional annotation of genetic variants from high-throughput sequencing data. Nucleic Acids Res. *38*, e164.

71. Landrum, M.J., Lee, J.M., Benson, M., Brown, G.R., Chao, C., Chitipiralla, S., Gu, B., Hart, J., Hoffman, D., Jang, W., et al. (2018). ClinVar: improving access to variant interpretations and supporting evidence. Nucleic Acids Res. *46*, D1062–D1067.

72. Richards, S., Aziz, N., Bale, S., Bick, D., Das, S., Gastier-Foster, J., Grody, W.W., Hegde, M., Lyon, E., Spector, E., et al. (2015). Standards and guidelines for the interpretation of sequence variants: a joint consensus recommendation of the American College of Medical Genetics and Genomics and the Association for Molecular Pathology. Genet. Med. *17*, 405–424.

73. Lee, S., Jang, S., Kim, J.I., Chae, J.H., Kim, K.J., and Lim, B.C. (2022). Whole genomic approach in mutation discovery of infantile spasms patients. Front. Neurol. *13*, 944905.

74. Cabarcas, S., Jacob, J., Veras, I., and Schramm, L. (2008). Differential expression of the TFIIIB subunits Brf1 and Brf2 in cancer cells. BMC Mol. Biol. *9*, 74.

75. Bandiera, R., Wagner, R.E., Britto-Borges, T., Dieterich, C., Dietmann, S., Bornelöv, S., and Frye, M. (2021). RN7SK small nuclear RNA controls bidirectional transcription of highly expressed gene pairs in skin. Nat. Commun. *12*, 5864.

76. Meng, Q., Xu, J., Liang, C., Liu, J., Hua, J., Zhang, Y., Ni, Q., Shi, S., and Yu, X. (2018). GPx1 is involved in the induction of protective autophagy in pancreatic cancer cells in response to glucose deprivation. Cell Death Dis. *9*, 1187.

77. Wei, S., Yu, Z., Shi, R., An, L., Zhang, Q., Zhang, Q., Zhang, T., Zhang, J., and Wang, H. (2022). GPX4 suppresses ferroptosis to promote malignant progression of endometrial carcinoma via transcriptional activation by ELK1. BMC Cancer *22*, 881.

78. Dobin, A., Davis, C.A., Schlesinger, F., Drenkow, J., Zaleski, C., Jha, S., Batut, P., Chaisson, M., and Gingeras, T.R. (2013). STAR: ultrafast universal RNA-seq aligner. Bioinformatics *29*, 15–21.

79. Li, B., and Dewey, C.N. (2011). RSEM: accurate transcript quantification from RNA-Seq data with or without a reference genome. BMC Bioinformatics *12*, 323.

80. Love, M.I., Huber, W., and Anders, S. (2014). Moderated estimation of fold change and dispersion for RNA-seq data with DESeq2. Genome Biol. *15*, 550.

81. Kolde, R. (2012). Pheatmap: pretty heatmaps. R package version *1*, 726.

82. Xie, Z., Bailey, A., Kuleshov, M.V., Clarke, D.J.B., Evangelista, J.E., Jenkins, S.L., Lachmann, A., Wojciechowicz, M.L., Kropiwnicki, E., Jagodnik, K.M., et al. (2021). Gene Set Knowledge Discovery with Enrichr. Curr. Protoc. *1*, e90.

83. Yoon, S.W., Kim, D.K., Kim, K.P., and Park, K.S. (2014). Rad51 regulates cell cycle progression by preserving G2/M transition in mouse embryonic stem cells. Stem Cells Dev. *23*, 2700–2711.

84. Neavin, D., Senabouth, A., Arora, H., Lee, J.T., Ripoll-Cladellas, A., sc-eQTLGen Consortium, Franke, L., Prabhakar, S., Ye, C.J., McCarthy, D.J., and Melé, M. (2024). Demuxafy: improvement in droplet assignment by integrating multiple single-cell demultiplexing and doublet detection methods. Genome Biol. *25*, 94.